A Feed-forward Pathway Drives LRRK2 kinase Membrane Recruitment and Apparent Activation

Edmundo G. Vides[1,3], Ayan Adhikari[1,3], Pawel Lis[2,3], Elena Purlyte[2,3], Justin Shumate[1,3], Elena Spinola Lasso[2,3], Herschel S. Dhekne[1,3], Dario R. Alessi[2,3], and Suzanne R. Pfeffer[1,3]*

[1]Department of Biochemistry, Stanford University School of Medicine

[2]MRC Protein Phosphorylation and Ubiquitylation Unit, University of Dundee

[3]Aligning Science Across Parkinson's (ASAP) Collaborative Research Network, Chevy Chase, MD

*Corresponding Author

Address:

279 Campus Drive

Stanford, California, USA 94305-5307

E-mail Address: pfeffer@stanford.edu

Abstract

Activating mutations in the Leucine Rich Repeat Kinase 2 (LRRK2) cause Parkinson's disease and previously we showed that activated LRRK2 phosphorylates a subset of Rab GTPases (Steger et al., 2017). Moreover, Golgi-associated Rab29 can recruit LRRK2 to the surface of the Golgi and activate it there for both auto- and Rab substrate phosphorylation. Here we define the precise Rab29 binding region of the LRRK2 Armadillo domain between residues 360-450 and show that this site, termed "Site #1", can also bind additional LRRK2 substrates, Rab8A and Rab10. Moreover, we identify a distinct, N-terminal, higher affinity interaction interface between LRRK2 phosphorylated Rab8 and Rab10 termed "Site #2", that can retain LRRK2 on membranes in cells to catalyze multiple, subsequent phosphorylation events. Kinase inhibitor washout experiments and mutation analysis demonstrate that rapid recovery of kinase activity in cells depends on the ability of LRRK2 to associate with phosphorylated Rab reaction products. Reconstitution of purified LRRK2 recruitment onto planar lipid bilayers decorated with Rab10 protein demonstrates cooperative association of only active LRRK2 with phospho-Rab10-containing membrane surfaces. These experiments reveal a feed-forward pathway that provides spatial control and apparent membrane activation of LRRK2 kinase activity.

Introduction

Activating mutations in the Leucine Rich Repeat Kinase 2 (LRRK2) cause inherited Parkinson's disease, and lead to the phosphorylation of a subset of Rab GTPases (Alessi and Sammler, 2018), in particular, Rab8A, Rab10, and Rab29 within a conserved residue of the Switch-II effector binding motif. Rab GTPases are master regulators of membrane trafficking and are thought to serve as identity determinants of membrane bound compartments of the secretory and endocytic pathways (Pfeffer, 2017). In their GTP bound forms, Rabs are best known for their roles in linking motor proteins to transport vesicles and facilitating the process of transport vesicle docking.

Our previous work showed that Rab phosphorylation blocks the ability of Rab proteins to be activated by their cognate guanine nucleotide exchange factors or to bind to the GDI proteins that recycle GDP-bearing Rabs from target membranes to their membranes of origin (Steger et al., 2016; 2017). Moreover, phosphorylation of Rab8A and Rab10 blocks their ability to bind known effector proteins and enhances binding to a novel set of effectors that includes RILPL1, RILPL2, JIP3, JIP4 and MyoVa proteins (Steger et al., 2017; Dhekne et al., 2021). Thus, Rab phosphorylation flips a switch on Rab effector selectivity that can drive dominant physiological changes, including blocking primary cilia formation (Steger et al., 2017; Dhekne et al., 2018; Sobu et al., 2021; Khan et al., 2021) and autophagosome motility in axons (Boecker et al., 2021).

Most LRRK2 is found in the cell cytosol where it appears to be inactive (Biskup et al., 2006; Berger et al., 2010; Purlyte et al., 2018). Recent structural analysis of the catalytic, C-terminal half of LRRK2 (Deniston et al., 2021) and full length human LRRK2 protein yielded structures of both monomeric and dimeric, inactive states (Myasnikov et al., 2021). Several groups have reported that active LRRK2 is a dimer (Greggio et al., 2008; Klein et al., 2009; Sen et al., 2009;

Berger et al, 2010; Civiero et al., 2012; Guaitoli et al, 2016), and higher order forms were detected on membranes upon crosslinking (Berger et al., 2010; Schapansky et al., 2014). Thus, LRRK2 membrane association is associated with kinase activation, however the molecular basis for this activation is not yet known.

Exogenously expressed, Golgi-localized Rab29 protein can recruit LRRK2 onto membranes and activate it there for both auto- and Rab substrate phosphorylation (Kuwahara et al., 2016; Liu et al., 2018; Purlyte et al., 2018; Madero-Pérez et al., 2018). Indeed, even Rab29 artificially anchored on mitochondria can activate LRRK2 and drive its membrane recruitment (Gomez et al., 2019). McGrath et al. (2021) implicated LRRK2 residues 386-392 as being important for the interaction of Rab29/32/38 family members with the LRRK2 kinase Armadillo domain. However, the LRRK2 Armadillo domain is located at some distance from the kinase domain, at least in the current structure models for LRRK2 protein (Myasnikov et al., 2021). Thus, how Rab29 binding might activate LRRK2 kinase activity is not at all clear. In addition, because Rab29 is not needed for LRRK2 action on Rab8A or Rab10 proteins (Kalogeropulou et al., 2020), other pathways for LRRK2 activation must exist.

In this study, we define a specific patch ("Site #1") of the LRRK2 Armadillo domain that binds to Rab8A, Rab10 and Rab29 protein with affinities similar to those reported previously (McGrath et al., 2021). More importantly, we identify a distinct region of LRRK2 Armadillo domain ("Site #2") that binds specifically to LRRK2-*phosphorylated* Rab8A and Rab10 proteins, to establish a feed forward activation mechanism for membrane-associated LRRK2 kinase.

Results

Rab29 binds to the C-terminal portion of the LRRK2 Armadillo domain

McGrath et al. (2021) showed that the LRRK2 Armadillo domain residues 1-552 contain a binding site that interacts specifically with purified Rab29, 32 and 38 in vitro with affinities of 2.7, 1.2 and 1.2-2.4μM, respectively. We used microscale thermophoresis to determine the affinity of other Rab GTPase substrates with this portion of LRRK2 kinase. For these experiments, portions of the LRRK2 Armadillo domain were fluorescently labeled and incubated with Rab GTPases in the presence of Mg^{++}-GTP. Figure 1 shows binding curves for Rab29 with full length Armadillo domain (residues 1-552, panel A), as well as sub-fragments composed of LRRK2 residues 1-159 (Fig. 1C) or 350-550 (Fig. 1D). Rab29 showed specific binding to the full length 1-552 Armadillo fragment with a K_D of 1.6μM (Fig. 1A), comparable to that reported previously using other methods (McGrath et al., 2021). No Rab29 binding was detected to a fragment representing the N-terminal 1-159 LRRK2 residues (binding >29μM; Fig. 1C); essentially full binding was observed with a fragment encompassing residues 350-550 (K_D = 1.6μM; Fig. 1D). Under these conditions, the non-LRRK2 substrate Rab7 protein failed to bind to the Armadillo 1-552 fragment (Fig. 1B). Thus, Rab29 binds to the C-terminal portion of LRRK2's Armadillo domain at a site we will refer to as Site #1.

Rab8A and Rab10 bind to the LRRK2 Armadillo domain

Similar experiments were carried out with Rab8A and Rab10, the most prominent LRRK2 substrates (Steger et al., 2017). Rab8A bound full length Armadillo domain with a K_D of 2.9μM (Fig. 2A), showed weaker interaction with the LRRK2 1-159 fragment (K_D ~ 6.7μM; Fig. 2B), and good binding to the 350-550 fragment (K_D = 2.3μM; Fig. 2C). These data indicate that Rab8A binds to the same site as Rab29. Like Rab8A, Rab10 bound to full length Armadillo 1-552 with a K_D of 2.4μM (Fig. 2D); weaker binding was detected for 1-159 and 350-550 fragments, yielding K_Ds of 5.1μM in both cases (Fig. 2E,F). Thus, in addition to Rab32, 38 and 29, Rabs

8A and 10 can bind to LRRK2 residues 350-550. Note that Rab32 and Rab38 are not substrates of LRRK2 kinase as they lack a phosphorylatable Ser/Thr residue in the Switch-II motif (Steger et al., 2016; 2107); they show extremely narrow tissue-specific expression but are related to Rab29 protein.

Residues critical for Rab GTPase binding to LRRK2 residues 350-550, Site #1

Previous work implicated LRRK2 residues 386–392 in contributing to a Rab29/32/38 binding interface (McGrath et al., 2021). We used a microscopy-based assay to identify any portions of the first 1000 residues of LRRK2 that would relocalize to the Golgi upon co-expression with Golgi localized, HA-Rab29 protein (Fig. 3-Fig. Suppl. 1). Twenty two constructs were transfected into cells and their localization scored visually. The smallest fragment of LRRK2 that interacted with HA-tagged Rab29 in HeLa cells, thereby co-localizing at the Golgi complex, encompassed LRRK2 residues 350-550.

We next deployed AlphaFold docking (Jumper et al., 2021) using ColabFold (Mirdita et al., 2021) and the AlphaFold2_advanced.ipynb notebook with the default settings to model the interaction of Rab29 with the LRRK2 350-550 fragment (Fig. 3A and Fig. 3-Fig. Suppl. 2). Residues highlighted in red show the most intimate contacts between LRRK2 and Rab29 and will be shown below to be essential for detection of this interaction in cells.

Three metrics were used to evaluate the importance of individual residues to contribute to Rab29 interaction. First, we tested the impact of mutations on the ability of full length LRRK2 to co-localize with HA-Rab29 at the Golgi in HeLa cells (Fig. 3B and Fig.3 – Fig. Suppl. 3); we also tested the ability of exogenously expressed Rab29 to stimulate activity of the same point mutants in the background of either wild type LRRK2 (Fig. 3C, Fig. 3–Fig. Suppl. 4A) or pathogenic R1441G LRRK2 (Fig. 3D, Fig 3.--Fig. Suppl. 4B). This work identified 4 key

mutations of highly conserved residues (R361E, R399E, L403A and K439E) that blocked both the co-localization of LRRK2 and Rab29 in HeLa cells (Fig. 3B, red) as well as activation of LRRK2 upon overexpression of Rab29 in HEK293 cells (Fig. 3C, red). In experiments undertaken with pathogenic R1441G LRRK2 that is more potently activated by Rab29, the K439E LRRK2 mutation completely blocked LRRK2 kinase activation; R399E showed weak activation (Fig. 3D and Fig. 3--Fig. Suppl. 4B). Some of the other mutants blocked co-localization with Rab29 in HeLa cells without completely suppressing LRRK2 activation following overexpression of Rab29. We therefore recommend using the K439E LRRK2 mutation to block Rab29 interaction and activation in future work (asterisks in Figs. 3B,C). Altogether, these data highlight the importance of a surface that is comprised of LRRK2 residues Arg361, Arg399, Leu403, Lys439 in binding Rab GTPases (Site #1) (Fig. 3A and Fig. 3 -Fig. Suppl. 2).

PhosphoRab binding to LRRK2, Site #2

To understand the consequences of LRRK2-mediated Rab GTPase phosphorylation, it is important to identify specific binding partners of phosphorylated Rab proteins, and to study the consequences of such binding events. We recently established a facile method that enables us to monitor phosphoRab binding to proteins of interest in conjunction with microscale thermophoresis binding assays (Dhekne et al., 2021; Vides and Pfeffer, 2021). Briefly, Rab proteins are phosphorylated in vitro by MST3 kinase that phosphorylates Rab proteins at the same position as LRRK2 kinase (Vieweg et al., 2020). Recombinant MST3 is much easier to purify in large amounts for biochemical experiments than LRRK2. We used this assay to monitor the possible interaction of phosphorylated LRRK2 substrates to the LRRK2 Armadillo domain, and were delighted to discover that pRab8A and pRab10 proteins bind with high affinity to a site distinct from that used by non-phosphorylated Rab proteins that we term site #2.

As shown in Fig. 4, phosphoRab8A and phosphoRab10 bound with K_Ds of ~900nM and 1μM to the full Armadillo domain 1-552 fragment, respectively (Figs. 4A, D); this binding reflected interaction with N-terminal LRRK2 residues 1-159, as this fragment was sufficient to yield essentially the same K_Ds of 1μM and 700 nM, respectively for phosphoRab8A and phosphoRab10 proteins (Figs. 4B, E). Furthermore, no binding was detected for phosphoRab8A or Rab10 with LRRK2 residues 350-550 (Figs. 4C, F). These data demonstrate that Rab8A and Rab10 GTPases, phosphorylated at the same residues modified by LRRK2 kinase bind very tightly to the LRRK2 N-terminus but no longer interact with the 350-550 region that interacts with dephosphorylated Rab proteins.

Electrostatic analysis of a model of the LRRK2 Armadillo domain revealed that the absolute N-terminus of LRRK2 contains a patch of basic amino acids (highlighted in blue) that may comprise a phosphoRab interaction interface (Fig. 5A) (Jurus et al., 2018; Pettersen et al., 2004). Such modeling led us to test the role of lysine residues at positions 17 and 18 in mediating LRRK2 interaction. Mutation of either lysine 17 or 18 abolished phosphoRab10 binding to LRRK2 Armadillo domain, with binding decreased to >20μM upon single mutation at either site (Fig. 5C, D). These lysine residues are highly conserved in evolution when analyzed using the Consurf server (Ashkenazy et al., 2016) with a conservation score of 2 for K17 and 8 for K18 (9 is the maximum score), indicating that K18 plays an especially important role. These experiments define a second, Rab binding site #2 that is specific for phosphorylated Rab proteins (Fig. 5B).

To determine the significance of the phosphoRab binding site in relation to LRRK2 membrane recruitment in cells, we generated full length FLAG-LRRK2 protein containing point mutations at both lysines 17 and 18 and investigated its cellular localization upon expression in HeLa cells (Fig. 6). To improve our ability to detect membrane associated LRRK2 distribution, cells grown

on collagen coated coverslips were dipped in liquid nitrogen and then thawed in a physiological, glutamate-containing buffer to crack open the plasma membrane and release cytosolic proteins prior to fixation (Seaman et al., 2004; Purlyte et al., 2018). Under these conditions, LRRK2 co-localizes with phosphorylated Rab proteins (Purlyte et al., 2018; Sobu et al., 2021).

As expected, PhosphoRab10 was detected as a bright spot adjacent to the mother centriole in HeLa cells (Fig. 6A), and the co-expressed, R1441G pathogenic mutant LRRK2 protein showed good co-localization with phosphoRab10 protein (Figs. 6A,C), as we have reported previously (Purlyte et al., 2018; Sobu et al., 2021). In contrast, although exogenously expressed, R1441G LRRK2 bearing K17/18/A mutations still generated a perinuclear, phosphoRab10-containing structure, LRRK2 displayed much less co-localization with the phosphoRab proteins or with membranes overall (Figs. 6B,C). These experiments show that K17 and K18 are important for exogenous LRRK2 membrane association with a pool of highly phosphorylated Rab10 protein. The importance of LRRK2's N-terminal lysine residues also suggests that caution may be in order when evaluating membrane interactions of LRRK2 tagged N-terminally with larger tags such as GFP that may hinder access to K17/K18.

PhosphoRab-LRRK2 interaction increases rates of kinase recovery

We next explored the relevance of phosphoRab binding to LRRK2's N-terminus in relation to the overall kinetics of Rab phosphorylation in cells. LRRK2-mediated Rab GTPase phosphorylation is a highly dynamic process that is counteracted by the action of PPM1H phosphatase (Berndsen et al., 2019); at steady state, only a small fraction of total Rab proteins are LRRK2-phosphorylated (Ito et al., 2016). The initial rate of kinase activity can be determined by monitoring the phosphorylation of Rab10 protein after washout of the LRRK2 inhibitor, MLi-2 (Ito et al., 2016; Kalogeropulou, 2020).

When HeLa cells were treated with 200nM MLi-2 for 1hr and then washed with culture medium, Rab10 was efficiently rephosphorylated by exogenous, FLAG-tagged, R1441G LRRK2 protein over the 2h time course evaluated (Fig. 7A, E). In contrast, cells expressing FLAG-R1441G LRRK2 bearing K17/18A mutations showed comparable total phosphoRab10 levels to begin with, but significantly slower re-phosphorylation (Fig 7B, E). Similar results were obtained in experiments comparing the re-activation of FLAG-tagged, wild type LRRK2 (Fig. 7C,F) with that of LRRK2 K17/18A (Fig. 7D,F). As reported previously (Ito et al., 2016), wild type LRRK2 recovery was more efficient than that of R1441G LRRK2. In summary, these experiments demonstrate that K17/K18 residues are important for efficient reactivation of LRRK2 after MLI-2 washout, consistent with their role in anchoring LRRK2 at sites adjacent to phosphorylation substrates.

Cooperative LRRK2 membrane recruitment on Rab-decorated planar lipid bilayers

Binding of phosphoRab reaction products to Site #2 at the N-terminus of LRRK2 (Fig. 5B) would set up a feed-forward process whereby the product of an initial phosphorylation reaction would enhance subsequent Rab GTPase phosphorylation by holding the enzyme on the surface of membranes that contain relevant Rab GTPase substrates. To confirm this possibility and to visualize the process directly, we established a planar lipid bilayer system that would enable us to monitor the interaction of fluorescently labeled, purified, full length LRRK2 kinase with membrane anchored Rab10 substrate (Adhikari et al., 2022). For this purpose, bilayers were formed on the surface of glass bottom chambers comprised of phospholipids of a composition similar to that found in the Golgi (65% DOPC, 29% DOPS, 1% PI(4)P (Thomas and Fromme, 2016)), mixed with 0.1% of the lipophilic tracer DiD dye and 5% DOGS-NTA [Ni^2] to to enable anchoring of C-terminally His-tagged Rab10 protein. Binding of fluorescently labeled, hyperactive R1441G LRRK2 was then visualized in real time using total internal reflection

(TIRF) light microscopy. Reactions were carried out in the presence of ATP, GTP and an ATP regenerating system to provide physiological conditions for the full length LRRK2 enzyme. Note that we routinely utilize R1441G LRRK2 because it is a highly active kinase in cells, although in vitro, R1441G LRRK2 displays the same level of Rab kinase activity as wild type LRRK2 (cf. Steger et al., 2017).

As shown in Figure 8A (red dots), fluorescent R1441G LRRK2 bound efficiently to lipid bilayers, only in the presence of pre-anchored Rab10 protein (compare with purple dots in 8B) and not when Rab11 protein was instead employed (Fig. 8B, green dots; movies 1-3). Importantly, almost no binding was observed with kinase inactive D2017A LRRK2 (Fig. 8A yellow dots, movie 4) (Steger et al., 2016). This indicates that Rab GTPase binding to Site #1 residues 361-451 (Fig. 3B) results in a low affinity interaction that is not sufficient to retain this inactive LRRK2 protein on the bilayer under these conditions (7nM LRRK2, 2.5 μM Rab10). Reactions containing the Type I MLi-2 inhibitor showed aggregation of the fluorescent LRRK2 protein, as has been seen in cells. Incubations containing the Type 2 inhibitor, GZD-824 (Tasegian et al., 2021) showed weak binding, consistent with a requirement for phosphoRab10 generation to support LRRK2 binding to Site #2's K17 and K18; however under these conditions, LRRK2 was not monodisperse and could not be analyzed further. Importantly, R1441G LRRK2 mutated at lysines 17 and 18 bound to a lower extent than R1441G LRRK2 (Fig. 8A, blue dots; movie 5), confirming their important role in binding to phosphorylated Rab8A and Rab10. It is noteworthy that the K17/K18 mutant protein showed higher binding than the D2017A mutant, suggesting that the non-phosphoRab binding Site #1 may be more accessible for binding in an active versus inactive LRRK2 protein conformation.

Analysis of the kinetics of LRRK2 binding as a function of Rab protein concentration showed clear, cooperative membrane association of R1441G LRRK2, consistent with a feed-forward

mechanism, as predicted from the in vitro Rab binding data (Fig. 8C). A nonlinear regression fit of the data indicated a Hill coefficient of 2.7, consistent with a positive, cooperative phenomenon. In summary, these data demonstrate that LRRK2 kinase is recruited to membranes and then held there by phosphorylated Rabs to increase subsequent Rab GTPase phosphorylation as part of a cooperative, feed-forward pathway.

Discussion

LRRK2 is ~90% cytosolic (Purlyte et al., 2019), and little was known about why membrane-associated LRRK2 appears to be much more active than the cytosolic pool of kinase. We have confirmed here that LRRK2 kinase relies upon substrate Rab GTPases to achieve membrane association, and revealed that LRRK2 utilizes two distinct Rab binding sites within its N-terminal Armadillo domain for this purpose. Site #1 (Fig. 5B) binds multiple, non-phosphorylated Rab substrates including Rab8A, Rab10 and Rab29, as well as the highly tissue specific- and non-substrate, Rab29-related, Rab32 and Rab38 proteins (Waschbüsch et al., 2014; McGrath et al., 2021). The second site (#2) is located at LRRK2's absolute N-terminus, at a significant distance from the kinase active site; this site shows strong preference for phosphorylated Rab8A and Rab10 proteins.

Figure 9 shows our current model for LRRK2 membrane recruitment. LRRK2 will interact reversibly with any one of the subset of Rab proteins that can bind to site #1. Rab29 shows the highest affinity for this site, but Rab8A can also bind with physiologically relevant affinity. Rab GTPases cluster in microdomains on distinct membrane surfaces (Pfeffer, 2017; Sönnichsen et al., 2000; DeRenzis et al., 2002; Barbero et al., 2002), thus this initial LRRK2 membrane association will bring the kinase in contact with other copies of the same substrate Rab proteins for phosphorylation. After an initial phosphorylation event, LRRK2 will then be held in place by bivalent association with one phosphorylated and one non-phosphorylated Rab protein. By

binding to the kinase reaction product, LRRK2 enhances its effective, local activity by increasing the probability with which it will encounter another substrate Rab protein.

Despite relatively similar affinities for their respective Rab binding partners, the phosphoRab-specific site appears to drive stable LRRK2 membrane association, as mutation of two key lysine residues strongly impacts co-localization of LRRK2 protein with phosphoRabs in cells. In addition, kinase activity leads to a much higher degree of LRRK2 association with planar lipid bilayers, despite the presence of binding Site #1 for non-phosphorylated-Rabs. Finally, K17/K18A LRRK2 that cannot bind to phosphorylated Rab proteins showed lower bilayer association in comparison with native LRRK2, confirming the importance of this interaction. LRRK2 phosphorylation of Rab GTPases is therefore required to form a new, additional interaction interface that greatly enhances the overall avidity of LRRK2 membrane association.

Whether dual Rab engagement of the Armadillo domain influences the overall architecture of the enzyme and/or active site is not yet known, but membrane association may enhance LRRK2 oligomerization and higher order structure formation. In this regard it is important to note that quantitative mass spectrometry indicates that Rab10 is present at ~600 times the copy number as LRRK2 in MEF cells and brain tissue (https://copica.proteo.info/#/copybrowse). Thus, if Rab10 is assumed to exist in cells at ~2-5μM (Itzhak et al., 2016), LRRK2 will be present overall at about 3-8nM. These are very close to the concentrations used in our in vitro reconstitution experiments. Future experiments will be needed to elucidate the precise molecular state of LRRK2 upon engagement with Rab GTPases at sites #1 and #2.

Nichols et al. (2007) reported a single family with two affected siblings harboring LRRK2 E10K mutations. These patients presented with classic Parkinson's disease symptoms at age 57 including bradykinesia, muscular rigidity, postural instability, and resting tremor. Compared with

46 G2019S LRRK2 patients in that study whose disease onset was on average, 63.5 years, the two siblings had a more severely disabling disease, as indicated by a higher Hoehn and Yahr assessment score (4 versus 2.5, where 5 represents confinement to bed or wheelchair unless aided). Our study provides a molecular explanation for how a mutation located far from the kinase or ROC-COR domains may cause Parkinson's disease. We predict that the E10K mutation increases LRRK2 phosphoRab binding and membrane association and may display an even higher apparent activity than the most common pathogenic G2019S mutation. This distinction would need to be evaluated under conditions of MLi-2 washout, as exogenous expression would mask this subtle mechanistic feature.

The ability of multiple Rab binding sites to anchor LRRK2 on membranes will make the kinase appear more active than the pool of cytosolic LRRK2 protein. Rab binding may also increase access of LRRK2 to other kinases that stabilize it in a more active conformation. Anchoring LRRK2's N-terminus may also influence autophosphorylation, which could also drive LRRK2 towards a more catalytically active conformation. Future structural studies of membrane anchored LRRK2 will provide important, additional information related to all of these possibilities.

Author contributions:
EGV: Experimentation for Figs. 1,2, 4-8
AA: Establishment of assay and Fig. 7,8
PL: Fig. 3 and Fig. 3 supplements
EP: Fig. 3 and Fig. 3 supplements
JS: Protein purification for Figs. 1, 2, 4
ESL: Fig. 3 and Fig. 3 supplements
HSD: Quantitation of Figure 3 and Figure 8 images
DRA and SRP: Supervising research, acquiring funding, writing/editing manuscript

KEY RESOURCES. Primary antibodies and reagents used in this study (available on request or from vendors)

KEY RESOURCES TABLE				
Reagent type (species) or resource	**Designation**	**Source or reference**	**Identifiers**	**Additional information**
bacterial strain	E. coli DH5α	Thermo Fisher	18258012	
bacterial strain	E. coli STBL3	Thermo Fisher	C737303	
bacterial strain	E. coli Rosetta DE3 pLys	Millipore	70956	
plasmid	pNIC Bsa-4 His-Sumo Rab10 Q68L 1-181	gift of Amir Khan		human
plasmid	pET15b His-Mst3	gift of Amir Khan		human
plasmid	pET21b GFP-Rab10 Q68L-His	Addgene in progress		human
plasmid	pET21b His Rab8A Q63L	Addgene in progress		human
plasmid	pQE-80L 2xHis-Rab29	Addgene in progress		human
plasmid	pQE-80L 2xHis-LRRK2 Armadillo 1-552	Addgene in progress		human
plasmid	pQE-80L 2xHis-LRRK2-Armadillo 1-159	Addgene in progress		human
plasmid	pQE-80L 2xHis-LRRK2-Armadillo 350-550	Addgene in progress		human
plasmid	pQE-80L 2xHis-LRRK2-Armadillo K17A	Addgene in progress		human
plasmid	pQE-80L 2xHis-LRRK2-Armadillo K18A	Addgene in progress		human
plasmid	pCMV5 FLAG-LRRK2 K17A/K18A/R1441G	Addgene in progress		human
plasmid	pCMV5 FLAG-LRRK2	MRC PPU Reagents and Services, U. Dundee	DU6841	human
plasmid	pCMV5 FLAG-LRRK2 R1441G	MRC PPU Reagents and Services, U. Dundee	DU13077	human
plasmid	pCMV5 FLAG-LRRK2 D2017A	MRC PPU Reagents and Services, U. Dundee	DU52725	human
recombinant protein	His Rab7	Addgene		
cell line	HeLa	ATCC	CCL-2	
cell line	HEK293T	ATCC	CRL-3216	
Antibody	anti-LRRK2 (mouse monoclonal)	Neuromab	N241A/34	(1:1000)
Antibody	anti-LRRK2 phospho S935 (rabbit monoclonal)	Abcam	UDD2	(1:1000)
Antibody	anti-Rab10 (mouse monoclonal)	Nanotools	0680–100/Rab10-605B11	(1:1000)
Antibody	anti-Rab10 (phospho T73) (rabbit monoclonal)	Abcam	ab230261	(1:1000)

Antibody	anti-FLAG M2 (mouse monoclonal)	Millipore Sigma	F-1804	(1:2000)
Affinity resin	FLAG M2 affinity gel	Millipore Sigma	A2220	
Chemical compound, drug	MLi-2	MRC PPU Reagents and Services, U. Dundee		
Commercial assay or kit	RED-NHS 2nd Generation (Amine Reactive) Protein Labeling Kit	Nanotemper Technologies	MO-L011	
Commercial assay or kit	CF® 633 Succinimidyl Ester Protein Labeling Kit	Biotium	#92217	
Software, Algorithm	FIJI	PMID: 29187165	RRID:SCR_002285	
Software, Algorithm	CellProfiler	PMID: 29969450	RRID:SCR_007358	
Software, Algorithm	TrackIt	PMID: 33947895		
Lipid	18:1 (Δ9-Cis) PC (DOPC)	Avanti Polar Lipids	#850375	11 µmol
Lipid	18:1 PS (DOPS)	Avanti Polar Lipids	#840035	5 µmol
Lipid	18:1 DGS-NTA(Ni)	Avanti Polar Lipids	#790404	0.85 µmol
Lipid	18:1 PI(4)P	Avanti Polar Lipids	#850151	0.15 µmol
Lipophilic tracer	DiD	Thermo Fischer	D7757	0.01 µmol
Chemical compund	Creatine Phosphate	Fluka Analytical	#27920	20mM
Enzyme	Creatine Phosphokinase	Sigma	C3755	30U

Methods

Cloning and plasmids

DNA constructs were amplified in Escherichia coli DH5α or STBL3 and purified using mini prep columns (Econospin). DNA sequence verification was performed by Sequetech (http://www.sequetech.com). pNIC Bsa-4 His-Sumo Rab10 Q68L 1-181 and pET15b His-Mst3 were kind gifts of Amir Khan (Harvard University). pET21b GFP-Rab10 Q68L-His was subcloned from GFP-Rab10 (Gomez et al. 2019) into pET21b. The C-terminal His tagged version was generated by Gibson assembly. His Rab8A Q63L was subcloned from HA-Rab8A (DU35414, Medical Research Council at Dundee) into pET14b. Point mutations were generated using site directed mutagenesis. His-Rab29 was subcloned from HA-Rab29 (DU5022, Medical Research Council at Dundee) into the pQE-80L backbone. pCMV5 FLAG-LRRK2 (DU6841), Flag-LRRK2 R1441G (DU13077), and FLAG-LRRK2 D2017A (DU52725) were obtained from the Medical Research Council at Dundee. His-Armadillo 1-552, 1-159, and 350-550 were all cloned from pCMV5 FLAG-LRRK2 into pQE-80L. K17A, K18A, and K17A/K18A LRRK2 and LRRK2 Armadillo were generated using site directed mutagenesis. All cloning and subcloning was done by Gibson assembly.

Rab GTPase, LRRK2 Armadillo domain, and LRRK2 purification

His Rab29, His Rab10-Q68L (1–181), His-Mst3, His-Rab8A Q63L, His-LRRK2 Armadillo (1-552), His-LRRK2 Armadillo (1-159), His-LRRK2 Armadillo (350-550), His-LRRK2 Armadillo K17A, and His-LRRK2 Armadillo K18A were purified in E.coli BL21 (DE3 pLys). Detailed protocols can be found in Gomez et al., 2020 and Vides et al., 2021. Bacterial cells were grown at 37°C in Lucia Broth medium and induced at A600 nm = 0.6–0.7 by the addition of 0.3 mM isopropyl-1- thio-β-D-galactopyranoside (Gold Biotechnology) and harvested after 18 h at 18°C. The cell pellets were resuspended in ice cold lysis buffer (50 mM HEPES, pH 8.0, 10% [vol/vol] glycerol, 500 mM NaCl,10 mM imidazole, 5 mM $MgCl_2$, 0.2mM tris(2-carboxyethyl)phosphine (TCEP), 20 μM GTP, and EDTA-free protease inhibitor cocktail (Roche). The resuspended bacteria were lysed by one passage through an Emulsiflex-C5 apparatus (Avestin) at 10,000 lbs/in^2 and centrifuged at 40,000 rpm for 45 min at 4°C in a Beckman Ti45 rotor. Cleared lysate was filtered through 0.2μm filter bottle (Nalgene) and passed over a HiTrap TALON crude 1mL column (Cytivia). The column was washed with lysis buffer until absorbance values reached pre-lysate loaded values. Protein was eluted with a gradient from 20-500 mM imidazole containing lysis buffer. Peak fractions were run on 10% SDS-PAGE gels to locate protein. The

eluate was buffer exchanged and further purified by gel filtration on Superdex-75 (GE Healthcare) with 50 mM HEPES, pH 8, 5% (vol/vol) glycerol, 150 mM NaCl, 5 mM $MgCl_2$, 0.1 mM tris(2-carboxyethyl) phosphine (TCEP), and 20 μM GTP. LRRK2 R1441G was transfected into HEK293T cells with Polyethylenimine HCl MAX 4000 (PEI) (Polysciences, Inc.) and purified 48hrs post transfection. Cells were lysed in 50mM Hepes pH 8, 150mM NaCl, 1mM EDTA, 0.5% Triton-X 100, 10% (vol/vol) glycerol and protease inhibitor cocktail (Roche). Lysate was centrifuged at 15,000g for 20min in Fiberlite F15 rotor (ThermoFischer). Clarified lysate was filtered through 0.2μm syringe filters and circulated over anti-FLAG M2 affinity gel (Sigma) at 4°C for 4hrs using a peristaltic pump. The affinity gel was washed with 6 column volumes of lysis buffer followed by 6 column volumes of elution buffer (50mM Hepes pH 8, 150mM NaCl, and 10% [vol/vol] glycerol). Protein was eluted from resin with 5 column volumes of FLAG peptide (0.25mg/mL) containing elution buffer. Eluate was supplemented to 20μM GTP, 1mM ATP, and 2mM $MgCl_2$.

In vitro Rab phosphorylation and microscale thermophoresis

A detailed method can be found on protocols.io (Vides et al., 2021). His-Rab10 Q63L 1–181 or His-Rab8A Q63L was incubated with His-Mst3 kinase at a molar ratio of 3:1 (substrate:kinase). The reaction buffer was 50 mM Hepes, pH 8, 5% (vol/vol) glycerol, 100 mM NaCl, 5 mM $MgCl_2$, 0.2 mM TCEP, 20 μM GTP, 5 μM BSA, 0.01% Tween-20, and 2 mM ATP (no ATP for negative control). The reaction mixture was incubated at 27°C for 30 min in a water bath. Phosphorylation completion was assessed by Western blot. Immediately after phosphorylation, the samples were transferred to ice before binding determination. See also Knebel et al., 2021.

Protein–protein interactions were monitored by microscale thermophoresis using a Monolith NT.115 instrument (Nanotemper Technologies). His LRRK2 Armadillo (1-552), (1-159), (350-550), K17A and K18A were labeled using RED-NHS 2nd Generation (Amine Reactive) Protein Labeling Kit (Nanotemper Technologies). For all experiments, the unlabeled protein partner was titrated against a fixed concentration of the fluorescently labeled LRRK2 Armadillo (100 nM); 16 serially diluted titrations of the unlabeled protein partner were prepared to generate one complete binding isotherm. Binding was carried out in a reaction buffer in 0.5-ml Protein LoBind tubes (Eppendorf) and allowed to incubate in the dark for 30 min before loading into NT.115 premium treated capillaries (Nanotemper Technologies). A red LED at 30% excitation power (red filter, excitation 605–645 nm, emission 680–685 nm) and IR-laser power at 60% was used for 30 s followed by 1 s of cooling. Data analysis was performed with NTAffinityAnalysis software (NanoTemper Technologies) in which the binding isotherms were derived from the raw

fluorescence data and then fitted with both NanoTemper software and GraphPad Prism to determine the K_D using a non-linear regression method. The binding affinities determined by the two methods were similar. Shown are averaged curves of Rab GTPase binding partners from single readings from two different protein preparations.

Cell culture and Immunoblotting

HEK293T and HeLa cells were obtained from American Type Culture Collection were cultured at 37°C and under 5% CO2 in Dulbecco's modified Eagle 's medium containing 10% fetal bovine serum, 2 mM Glutamine, and penicillin (100 U/ml)/streptomycin (100 µg/ml). HEK293T and HeLa cells were transfected with polyethylenimine HCl MAX 4000 (Polysciences). Cells were routinely checked for Mycoplasma by PCR analysis.

HeLa cells for pRab10 recovery kinetics were lysed 48 hr post transfection and MLi-2 treatment in ice cold lysis buffer (50mM Tris pH 7.4, 150mM NaCl, 0.5% Triton X-100, 5mM $MgCl_2$, 1 mM sodium orthovanadate, 50 mM NaF, 10 mM 2-glycerophosphate, 5 mM sodium pyrophosphate, 0.1 µg/ml mycrocystin-LR (Enzo Life Sciences), and EDTA-free protease inhibitor cocktail (Sigma-Aldrich). Lysates were centrifuged at 14,000g for 15 min at 4°C and supernatant protein concentrations were determined by Bradford assay (Bio-Rad).

A detailed protocol for blotting is available on protocols.io (Tonelli and Alessi, 2021). 20µg of protein were run on SDS PAGE gels and transferred onto nitrocellulose membranes using a Bio-Rad Trans-turbo blot system. Membranes were blocked with 2% BSA in Tris-buffered saline with Tween-20 for 30 at RT. Primary antibodies used were diluted in blocking buffer as follows: mouse anti-LRRK2 N241A/34 (1:1000, Neuromab); rabbit anti-LRRK2 phospho S935 (1:1000, Abcam); mouse anti-Rab10 (1:1000, Nanotools); and rabbit anti-phospho Rab10 (1:1000, Abcam). Primary antibody incubations were done overnight at 4°C. LI-COR secondary antibodies diluted in blocking buffer were 680 nm donkey anti-rabbit (1:5,000) and 800 nm donkey anti-mouse (1:5,000). Secondary antibody incubations were for 1 h at RT. Blots were imaged using an Odyssey Infrared scanner (LI-COR) and quantified using ImageJ software.

MLi-2 washout/ pRab10 recovery kinetics

HeLa cell seeded in 6x 60mm dishes expressing FLAG-LRRK2, LRRK2 K17A/K18A, LRRK2 R1441G, or LRRK2 R1441G/K17A/K18A for 48 hours were incubated with 200nm MLi-2 or DMSO for 1 hour under normal growth conditions at 37°C. To remove the MLi-2 inhibitor, cells

were washed 4 times with complete media. Washouts were done to allow for 120-15 min of enzyme activity recovery; after which, cells were harvested.

Confocal light microscopy

The standard method to obtain images in Figure 3 and Figure 3 supplements can be found on protocols.io (Purlyte et al., 2022). For Figure 8, cells were plated onto collagen coated coverslips with indicated plasmids. Cells were washed with ice cold phosphate buffered saline (PBS) 3x. After, they were incubated in glutamate buffer (25mM KCl, 25mM Hepes pH7.4, 2.5mM magnesium acetate, 5mM EGTA, and 150mM K glutamate) for 5 min on ice. Coverslips were dipped into liquid nitrogen and held for 5 sec before removal. They were thawed at RT, incubated in glutamate buffer for 2 min and then in PBS for 5 min. Cells were fixed with 3.5% paraformaldehyde in PBS for 15 min, permeabilized for 3 min in 0.1% Triton X-100, and blocked with 1% BSA in PBS. Antibodies were diluted as follows: mouse anti-FLAG (1:2000, Sigma-Aldrich) and rabbit anti pRab10 (1:2000; Abcam). Highly cross-absorbed H+L secondary anti-bodies (Life Technologies) conjugated to Alexa Fluor 568 or 647 were used at 1:2,000. Images were obtained using a spinning disk confocal microscope (Yokogawa) with an electron multiplying charge coupled device camera (Andor) and a 100× 1.4 NA oil immersion objective. Mander's correlation coefficients were calculated by analyzing maximum intensity projection images with CellProfiler software (Carpenter et al., 2006; Stirling et al., 2021).

Co-localization of Rab29 with full length LRRK2 and its mutants was quantified using an unbiased Cellprofiler pipeline as follows: Step 1. Imported raw .lsm files; 2. metadata extracted from the file headers; 3. images grouped by mutations and split into 3 channels; 4. nuclei identified as primary objects after rescaling intensities; 5. Nucleus is defined as the primary object and cells are identified by 'propagation' as secondary objects; cells are identified as the using the rescaled and smoothened LRRK2 channel. 6. Co-localization within whole cells is measured by thresholded (10) Mander's coefficient on the entire batch of images. Data plotted from Cellprofiler are relative values.

Substrate supported lipid bilayer preparation

A detailed method can be found on protocols.io (Adhikari et al., 2022). Briefly, we used Lab-TeKII 8 chambered No. 1.5 borosilicate cover glasses (Fischer) for LRRK2 recruitment assays. Reactions chambers were cleaned by 30 min incubation in Piranha solution (1:3 [vol/vol] ratio of

30% H_2O_2 and 98% H_2SO_4) and extensive washing in Milli-Q water. The reaction chambers were stored in Milli-Q water for up to 2 weeks. Before use, reaction chambers were dried and further cleaned in a Harrick Plasma PDC-32C plasma cleaner for 10 min at 18W under ambient air.

We prepared substrate supported lipid bilayers on glass coverslips with 65% DOPC, 29% DOPS, 5% DOGS-NTA[Ni^2], 1% PI(4)P, 0.01% DIL (Avanti Polar Lipids;Thermo). The lipid mixture was suspended in 1ml chloroform and then dried under nitrogen flow in a glass vial and kept under vacuum for at least 1 h. The dried lipids were hydrated in SLB buffer (20 mM Hepes pH 8, 150 mM potassium acetate, 1 mM $MgCl_2$) by vortexing to produce multilamellar vesicles (MLVs). SUVs were prepared by bath sonication followed by extrusion through 100 nm polycarbonate membrane 21 times (Avestin). The produced SUVs were stored at -20°C. The supported lipid bilayer was formed in cleaned reaction chambers on glass surfaces by addition of liposomes to a final concentration of 5mM liposomes in SLB buffer. SUV fusion was induced by addition of 1mM $CaCl_2$ and incubated for 45 min at 37°C. Next, the unfused vesicles were washed with Milli-Q water and STD buffer (20mM Hepes pH 8, 150mM NaCl, 5mM $MgCl_2$).

Poly-D-lysine coating

Lab-TeKII 8 chambered No. 1.5 borosilicate coverglass (Fisher) were used for Poly-D-lysine coating experiments. 10 mg Poly-D-lysine (MPBio # SKU:02150175-CF) was dissolved in 1ml of sterile Milli-Q water as a 1% stock solution. The stock solution was then diluted two fold in PBS as 1X coating solution. Coating solution (200µl) was added to the reaction chamber and incubated for 5 min at 37°C. The coating solution was then removed by rinsing the chamber thoroughly with sterile Milli-Q water and equilibrated with reaction buffer.

TIRF microscopy

A detailed method can be found on protocols.io (Adhikari et al., 2022). All LRRK2 recruitment movies were obtained at 25°C, at a frame rate capture interval of 1 sec using a Nikon Ti-E inverted microscope with the Andor iXon+EMCCD camera model DU885 with PerfectFocus and a Nikon TIRF Apo 100x 1.46 NA oil immersion objective. The imaging was done with 300 EM camera gain and 50 ms exposure time with 200µW laser intensity. We analyzed the microscopy data with TrackIt (Kuhn T., et al., 2021) to obtain spot density of bound LRRK2.

Rab10-dependent LRRK2 recruitment

A detailed method can be found on protocols.io (Adhikari et al., 2022). Purified FLAG LRRK2 is labeled with CF633 succinimidyl ester (Biotium) by incubation with dye for 1 hr at RT in the dark. After dye removal using Pierce Dye Removal Columns (Thermo Scientific #22858), protein was determined by Bradford Assay. Labeling efficiency was determined using the dye extinction coefficient and preps were labeled with 2-3 moles of dye per mole LRRK2 for all experiments.

GFP Rab10 Q63L C-terminal His was added to supported lipid bilayers at a final concentration of 2.5μM in STD buffer and incubated for 20 min at 37°C. After incubation, Rab coated supported lipid bilayers were washed with STD buffer and then equilibrated with reaction buffer (20mM Hepes pH 8, 150mM NaCl, 5mM $MgCl_2$, 4mM ATP, 20μM GTP, 20mM creatine phosphate, 30U creatine phosphokinase). 14nM CF633-FLAG LRRK2 was prepared in reaction buffer and allowed to equilibrate to RT for 5 min. 40 sec into imaging, 100μL from the 200uL in the reaction chamber was removed. At 60 sec, 100μL of 14nM CF FLAG LRRK2 was added and imaged for 600 sec and for 300 sec for no Rab10 control.

Acknowledgements

This study was funded by the joint efforts of The Michael J. Fox Foundation for Parkinson's Research (MJFF) [17298 & 6986 (S.R.P. & D.R.A.)] and Aligning Science Across Parkinson's (ASAP) initiative. MJFF administers the grant (ASAP-000463, S.R.P. & D.R.A.) on behalf of ASAP and itself. Funds were also provided by the Medical Research Council [grant no. MC_UU_00018/1 (D.R.A.)] and the pharmaceutical companies supporting the Division of Signal Transduction Therapy Unit (Boehringer-Ingelheim, GlaxoSmithKline, Merck KGaA (D.R.A.).

For the purpose of open access, the authors have applied a CC-BY public copyright license to the Author Accepted Manuscript version arising from this submission. All primary data associated with each figure has been deposited in the Dryad repository and can be found at **https://doi.org/XXXXX/dryad.XXX**. We are especially grateful to Dr. Gheorghe Chistol for helpful discussion.

References

Adhikari, A, Vides, E. and Pfeffer, S.R. 2022. Reconstitution of LRRK2 membrane recruitment onto planar lipid bilayers. Protocols.io in process.

Alessi DR, Sammler E. LRRK2 kinase in Parkinson's disease. Science. 2018 Apr 6;360(6384):36-37. doi: 10.1126/science.aar5683.

Ashkenazy H, Abadi S, Martz E, Chay O, Mayrose I, Pupko T, Ben-Tal N. ConSurf 2016: an improved methodology to estimate and visualize evolutionary conservation in macromolecules. Nucleic Acids Res. 2016 Jul 8;44(W1):W344-50.

Barbero P, Bittova L, Pfeffer SR. Visualization of Rab9-mediated vesicle transport from endosomes to the trans-Golgi in living cells. J Cell Biol. 2002 Feb 4;156(3):511-8

Berger Z, Smith KA, Lavoie MJ. Membrane localization of LRRK2 is associated with increased formation of the highly active LRRK2 dimer and changes in its phosphorylation. Biochemistry. 2010 Jul 6;49(26):5511-23.

Berndsen K, Lis P, Yeshaw WM, Wawro PS, Nirujogi RS, Wightman M, Macartney T, Dorward M, Knebel A, Tonelli F, Pfeffer SR, Alessi DR. PPM1H phosphatase counteracts LRRK2 signaling by selectively dephosphorylating Rab proteins. Elife. 2019 Oct 30;8:e50416. doi: 10.7554/eLife.50416.

Biskup S, Moore DJ, Celsi F, Higashi S, West AB, Andrabi SA, Kurkinen K, Yu SW, Savitt JM, Waldvogel HJ, Faull RL, Emson PC, Torp R, Ottersen OP, Dawson TM, Dawson VL. Localization of LRRK2 to membranous and vesicular structures in mammalian brain. Ann Neurol. 2006 Nov;60(5):557-69.

Boecker CA, Goldsmith J, Dou D, Cajka GG, Holzbaur ELF. Increased LRRK2 kinase activity alters neuronal autophagy by disrupting the axonal transport of autophagosomes. Curr Biol. 2021 May 24;31(10):2140-2154.e6.

Civiero L, et al. (2012) Biochemical characterization of highly purified leucine-rich repeat kinases 1 and 2 demonstrates formation of homodimers. PLoS One 7(8):e43472.

de Renzis S, Sönnichsen B, Zerial M. Divalent Rab effectors regulate the sub-compartmental organization and sorting of early endosomes. Nat Cell Biol. 2002 Feb;4(2):124-33.

Deniston CK, Salogiannis J, Mathea S, et al. Structure of LRRK2 in Parkinson's disease and model for microtubule interaction. *Nature*. 2020;588(7837):344-349. doi:10.1038/s41586-020-2673-2

Dhekne HS, Yanatori I, Gomez RC, et al. A pathway for Parkinson's Disease LRRK2 kinase to block primary cilia and Sonic hedgehog signaling in the brain. *Elife*. 2018;7:e40202. Published 2018 Nov 6. doi:10.7554/eLife.40202

Dhekne HS, Yanatori I, Vides EG, Sobu Y, Diez F, Tonelli F, Pfeffer SR. LRRK2-phosphorylated Rab10 sequesters Myosin Va with RILPL2 during ciliogenesis blockade. Life Sci Alliance. 2021 Mar 16;4(5):e202101050. doi: 10.26508/lsa.202101050.

Tonelli, F and Alessi D. 2021. Quantitative Immunoblotting Analysis of LRRK2 Signalling Pathway. **Protocols.io** https://dx.doi.org/10.17504/protocols.io.bsgrnbv6

Gomez RC, Wawro P, Lis P, Alessi DR, Pfeffer SR. Membrane association but not identity is required for LRRK2 activation and phosphorylation of Rab GTPases. J Cell Biol. 2019 Dec 2;218(12):4157-4170.

Gomez RC, Vides EG, Suzanne Pfeffer 2020. Rab29 fast exchange mutants: characterization of a challenging Rab GTPase. **protocols.io** https://dx.doi.org/10.17504/protocols.io.bffrjjm6

Greggio E, Zambrano I, Kaganovich A, Beilina A, Taymans JM, Daniels V, Lewis P, Jain S, Ding J, Syed A, Thomas KJ, Baekelandt V, Cookson MR. The Parkinson disease-associated leucine-rich repeat kinase 2 (LRRK2) is a dimer that undergoes intramolecular autophosphorylation. The Journal of biological chemistry. 2008;283:16906–16914.

Guaitoli G, Raimondi F, Gilsbach BK, Gómez-Llorente Y, Deyaert E, Renzi F, Li X, Schaffner A, Jagtap PK, Boldt K, von Zweydorf F, Gotthardt K, Lorimer DD, Yue Z, Burgin A, Janjic N, Sattler M, Versées W, Ueffing M, Ubarretxena-Belandia I, Kortholt A, Gloeckner CJ. Structural model of the dimeric Parkinson's protein LRRK2 reveals a compact architecture involving distant interdomain contacts. Proc Natl Acad Sci U S A. 2016 Jul 26;113(30):E4357-66.

Ito G, Katsemonova K, Tonelli F, Lis P, Baptista MA, Shpiro N, Duddy G, Wilson S, Ho PW, Ho SL, Reith AD, Alessi DR. Phos-tag analysis of Rab10 phosphorylation by LRRK2: a powerful assay for assessing kinase function and inhibitors. Biochem J. 2016 Sep 1;473(17):2671-85.

Itzhak DN, Tyanova S, Cox J, Borner GH. Global, quantitative and dynamic mapping of protein subcellular localization. *Elife*. 2016;5:e16950. Published 2016 Jun 9. doi:10.7554/eLife.16950

Jumper J, Evans R, Pritzel A, Green T, Figurnov M, Ronneberger O, Tunyasuvunakool K, Bates R, Žídek A, Potapenko A, Bridgland A, Meyer C, Kohl SAA, Ballard AJ, Cowie A, Romera-Paredes B, Nikolov S, Jain R, Adler J, Back T, Petersen S, Reiman D, Clancy E, Zielinski M, Steinegger M, Pacholska M, Berghammer T, Bodenstein S, Silver D, Vinyals O, Senior AW, Kavukcuoglu K, Kohli P, Hassabis D. Highly accurate protein structure prediction with AlphaFold. Nature. 2021 Aug;596(7873):583-589.

Jurrus E, Engel D, Star K, Monson K, Brandi J, Felberg LE, Brookes DH, Wilson L, Chen J, Liles K, Chun M, Li P, Gohara DW, Dolinsky T, Konecny R, Koes DR, Nielsen JE, Head-Gordon T, Geng W, Krasny R, Wei G-W, Holst MJ, McCammon JA, Baker NA. Improvements to the APBS biomolecular solvation software suite. Protein Sci. 2018 Aug 24; 27 (1): 112-128.

Kalogeropulou AF, Freemantle JB, Lis P, Vides EG, Polinski NK, Alessi DR. Endogenous Rab29 does not impact basal or stimulated LRRK2 pathway activity. Biochem J. 2020 Nov 27;477(22):4397-4423.

Klein CL, Rovelli G, Springer W, Schall C, Gasser T, Kahle PJ. Homo- and heterodimerization of ROCO kinases: LRRK2 kinase inhibition by the LRRK2 ROCO fragment. J Neurochem 2009 Nov;111(3):703-15

Khan SS, Sobu Y, Dhekne HS, et al. Pathogenic LRRK2 control of primary cilia and Hedgehog signaling in neurons and astrocytes of mouse brain. *Elife*. 2021;10:e67900. Published 2021 Oct 18. doi:10.7554/eLife.67900

Knebel A, Berndsen K, Lis P, Alessi DR. 2021. Expression and purification of Rab10 (1-181) stoichiometrically phosphorylated at Thr73 (the LRRK2 site). protocols.io https://dx.doi.org/10.17504/protocols.io.bvjxn4pn

Kuhn T, Hettich J, Davtyan R, Gebhardt JCM. (2021) Single molecule tracking and analysis framework including theory-predicted parameter settings. *Sci Rep.* 11(1):9465.

Kuwahara T, Inoue K, D'Agati VD, Fujimoto T, Eguchi T, Saha S, Wolozin B, Iwatsubo T, Abeliovich A. 2016. LRRK2 and RAB7L1 coordinately regulate axonal morphology and lysosome integrity in diverse cellular contexts. *SciRep* 6:29945

Liu Z, Bryant N, Kumaran R, et al. LRRK2 phosphorylates membrane-bound Rabs and is activated by GTP-bound Rab7L1 to promote recruitment to the trans-Golgi network. Hum Mol Genet. 2018;27:385–395.

Madero-Pérez J, Fernández B, Lara Ordóñez AJ, Fdez E, Lobbestael E, Baekelandt V, Hilfiker S. RAB7L1-Mediated Relocalization of LRRK2 to the Golgi Complex Causes Centrosomal Deficits via RAB8A. Front Mol Neurosci. 2018 Nov 13;11:417.

McGrath E, Waschbüsch D, Baker BM, Khan AR. LRRK2 binds to the Rab32 subfamily in a GTP-dependent manner via its armadillo domain. Small GTPases. 2021 Mar;12(2):133-146.

McQuin C, Goodman A, Chernyshev V, Kamentsky L, Cimini BA, Karhohs KW, Doan M, Ding L, Rafelski SM, Thirstrup D, Wiegraebe W, Singh S, Becker T, Caicedo JC, Carpenter AE (2018). CellProfiler 3.0: Next-generation image processing for biology. PLoS Biol. 16(7):e2005970.

Mirdita M, Schütze K, Moriwaki Y, Heo L, Ovchinnikov S, Steinegger M. bioRxiv 2021.08.15.456425; doi: https://doi.org/10.1101/2021.08.15.456425

Myasnikov A, Zhu H, Hixson P, Xie B, Yu K, Pitre A, Peng J, Sun J. Structural analysis of the full-length human LRRK2. Cell. 2021 Jun 24;184(13):3519-3527.e10.

Nichols WC, Elsaesser VE, Pankratz N, Pauciulo MW, Marek DK, Halter CA, Rudolph A, Shults CW, Foroud T; Parkinson Study Group-PROGENI Investigators. LRRK2 mutation analysis in Parkinson disease families with evidence of linkage to PARK8. Neurology. 2007 Oct 30;69(18):1737-44.

Pettersen EF, Goddard TD, Huang CC, Couch GS, Greenblatt DM, Meng EC, Ferrin TE. UCSF Chimera--a visualization system for exploratory research and analysis. *J Comput Chem.* 2004 Oct;25(13):1605-12.

Pfeffer SR. Rab GTPases: master regulators that establish the secretory and endocytic pathways. Mol Biol Cell. 2017 Mar 15;28(6):712-715.

Purlyte E, Dhekne HS, Sarhan AR, et al. Rab29 activation of the Parkinson's disease-associated LRRK2 kinase. Embo J. 2018;37:1–18.

Purlyte E, Kalogeropulou A, Tonelli F, Alessi DR 2022. Immunofluorescence-based assay to assess LRRK2 association with microtubules in HEK293 cells. **protocols.io**https://dx.doi.org/10.17504/protocols.io.b5jhq4j6

Schapansky J, Nardozzi JD, Felizia F, LaVoie MJ. Membrane recruitment of endogenous LRRK2 precedes its potent regulation of autophagy. Hum Mol Genet. 2014 Aug 15;23(16):4201-14.

Seaman MN (2004) Cargo-selective endosomal sorting for retrieval to the Golgi requires retromer. J Cell Biol 165: 111–122

Sen S, Webber PJ, West AB (2009) Dependence of leucine-rich repeat kinase 2 (LRRK2) kinase activity on dimerization. J Biol Chem 284(52):36346–36356.

Sobu Y, Wawro PS, Dhekne HS, Yeshaw WM, Pfeffer SR. Pathogenic LRRK2 regulates ciliation probability upstream of tau tubulin kinase 2 via Rab10 and RILPL1 proteins. Proc Natl Acad Sci U S A. 2021 Mar 9;118(10):e2005894118.

Sönnichsen B, De Renzis S, Nielsen E, Rietdorf J, Zerial M. Distinct membrane domains on endosomes in the recycling pathway visualized by multicolor imaging of Rab4, Rab5, and Rab11. J Cell Biol. 2000 May 15;149(4):901-14.

Steger M, Diez F, Dhekne HS, Lis P, Nirujogi RS, Karayel O, Tonelli F, Martinez TN, Lorentzen E, Pfeffer SR, Alessi DR, Mann M. Systematic proteomic analysis of LRRK2-mediated Rab GTPase phosphorylation establishes a connection to ciliogenesis. Elife. 2017 Nov 10;6:e31012.

Steger M, Tonelli F, Ito G, Davies P, Trost M, Vetter M, Wachter S, Lorentzen E, Duddy G, Wilson S, Baptista MA, Fiske BK, Fell MJ, Morrow JA, Reith AD, Alessi DR, Mann M. Phosphoproteomics reveals that Parkinson's disease kinase LRRK2 regulates a subset of Rab GTPases. Elife. 2016 Jan 29;5:e12813.

Stirling DR, Swain-Bowden MJ, Lucas AM, Carpenter AE, Cimini BA, Goodman A (2021). CellProfiler 4: improvements in speed, utility and usability. BMC Bioinformatics, 22 (1), 433.

Tasegian A, Singh F, Ganley IG, Reith AD, Alessi DR. Impact of Type II LRRK2 inhibitors on signaling and mitophagy. Biochem J. 2021 Oct 15;478(19):3555-3573.

Thomas LL, Fromme JC. 2016. GTPase cross talk regulates TRAPPII activation of Rab11 homologues during vesicle biogenesis. J Cell Biol. 215(4):499-513.

Tonelli, F and Alessi D. 2021. Quantitative Immunoblotting Analysis of LRRK2 Signalling Pathway. **Protocols.io** https://dx.doi.org/10.17504/protocols.io.bsgrnbv6

Vides EG, Pfeffer SR 2021. Microscale Thermophoresis determination of Rab29 binding to LRRK2 Armadillo Domain. Protocols.io https://dx.doi.org/10.17504/protocols.io.bvvmn646

Viewegg S, Mulholland K, Brauning B, Kachariya N, Lai Y, Toth R, Kishor Singh R, Volpi I, Sattler M, Groll M, Itzen A, Muqit MMK. PINK1-dependent phosphorylation of Serine111 within the SF3 motif of Rab GTPases impairs effector interactions and LRRK2-mediated phosphorylation at Threonine72. Biochem J. 2020 May 15; 477(9):1651-1668.

Waschbüsch D, Michels H, Strassheim S, Ossendorf E, Kessler D, Gloeckner CJ, et al. (2014) LRRK2 Transport Is Regulated by Its Novel Interacting Partner Rab32. PLoS ONE 9(10): e111632.

Figure Legends

Figure 1. Rab29 binds to the C-terminal portion of the LRRK2 Armadillo domain.

Microscale thermophoresis of full length (residues 1-552), labeled LRRK2 Armadillo

domain with Rab29 (A) or with Rab7 (B). (C, D) Microscale thermophoresis of labeled LRRK2 Armadillo domain residues 1-159 (C) or 350-550 (D) with Rab29. Purified Rab29 was serially diluted and then NHS-RED labeled-LRRK2 Armadillo (final concentration 100nM) was added. Graphs show mean and SEM from three independent measurements, each from a different set of protein preparations.

Figure 2. Rab8A and Rab10 bind to the LRRK2 Armadillo domain. (A-C) Microscale thermophoresis of labeled, LRRK2 Armadillo domain fragments comprised of residues 1-552, 1-159, or 350-550 with Rab8A as indicated. (C, D, E) Microscale thermophoresis for Rab10 with indicated LRRK2 Armadillo fragments, as in A. Purified Rab8A or Rab10 was serially diluted and then NHS-RED labeled LRRK2 Armadillo domain (final concentration 100nM) was added. Graphs show mean and SEM from three independent measurements, each from a different set of protein preparations.

Figure 3. Characterization of critical LRRK2 residues mediating binding to Rab29. (A) Predicted interactions between Rab29 and the LRRK2 Armadillo domain using AlphaFold docking (Jumper et al., 2021), ColabFold (Mirdita et al., 2021) and the AlphaFold2_advanced.ipynb notebook default settings. Residues shown in red show the most intimate and key contacts between LRRK2 and Rab29. (B) The wild type and indicated mutants of full length of GFP-LRRK2 were co-expressed with HA-Rab29 in HeLa cells. 24h post transfection cells were fixed and localization assessed by confocal microscopy. LRRK2 overlap with Rab29 is presented as a Mander's coefficient determined using Cellprofiler software (McQuin et al., 2018). (C) Wild type and indicated mutants of full length of GFP-LRRK2 were co-expressed with HA-Rab29 in HEK293T cells. 24h post transfection, cells were lysed and extracts immunoblotted with the

indicated antibodies. Shown is the average and standard deviation of duplicate determinations.

Figure 3 Figure Supplement 1. (top) Fragments of GFP-LRRK2 that were co-expressed with HA-Rab29 in HeLa cells. 24h post transfection, cells were fixed and localization assessed by confocal microscopy. Fragments that co-localized with Rab29 at the Golgi are shown in green and those that failed to co-localize in gray. The smallest fragment of LRRK2 that co-localized with Rab29 encompassed residues 350-550 (shown below). Magnification bar, 20μm.

Figure 3 Figure Supplement 2. (A) Alphafold model of Rab29 (grey) bound to the 350-550 fragment of LRRK2 (purple) as in Fig. 3A. (B) Table of Site #1 residues predicted to lie within the interface of LRRK2 and Rab29. Highlighted in red are residues that when mutated, suppress interaction of LRRK2 with Rab29 and inhibit Rab29-mediated LRRK2 activation in cells.

Figure 3 Figure Supplement 3. Examples of micrographs used to create Fig. 3B. Mutants (indicated) of full length GFP-LRRK2 were co-expressed with HA-Rab29 in HeLa cells. 24h post transfection, cells were fixed and localization assessed by confocal microscopy. Magnification bar, 20μm.

Figure 3 –Figure Supplement 4. Immunoblots used to obtain Fig. 3C and Fig. 3D. Wild type and indicated mutants of full length of GFP-LRRK2 (A) or R1441G LRRK2 (B) were co-expressed with HA-Rab29 in HEK293T cells. 24h post transfection cells were fixed and samples analyzed for immunoblotting.

Figure 4. phosphoRab8A and phosphoRab10 bind with high affinity to the N-terminal portion of the LRRK2 Armadillo domain. (A-F) Microscale thermophoresis of labeled, indicated, LRRK2 Armadillo fragments with phosphoRab8A (A-C) or with phosphoRab10 (pRab10 (D-F). Purified Rab proteins were phosphorylated with Mst3 kinase at 27°C for 2 h and then serially diluted; NHS-RED labeled Armadillo (final concentration 100 nM) was then added. Graphs show mean and SEM from three independent measurements, each from a different set of protein preparations.

Figure 5. A. Electrostatic surface potential of LRRK2 Armadillo domain residues 1-552 modeled using Chimera 2 software (Petterson et al., 2004); blue indicates a positively charged surface. LRRK2 K17 and K18 are indicated. (B) Alphafold (Jumper et al., 2021) structure of putative, active LRRK2 with residues that mediate Rab29 binding shown in red (Site #1) and the K17/K18 residues that are required for phosphoRab10 binding (Site #2) shown in magenta; the kinase domain is shown in blue. (C,D) Microscale thermophoresis of labeled, full length LRRK2 K17A or K18A Armadillo 1-552 with phosphoRab10. Purified Rab10 protein was phosphorylated with Mst3 kinase at 27°C for 2 h and then serially diluted; NHS-RED labeled Armadillo (final concentration 100 nM) was then added. Graphs show mean and SEM from three independent measurements, each from a different set of protein preparations.

Figure 6. LRRK2 K17 and K18 are critical for pRab10 interactions in cells. (A) FLAG-LRRK2 R1441G (red) was transfected into HeLa cells plated on collagen coated coverslips and co-localized with pRab10 (green). Cells on coverslips were dipped in liquid nitrogen to deplete cytosol and enhance membrane-bound signal. Insets show enlargements of boxed areas representing peri-centriolar LRRK2 and pRab10. (B)

FLAG-LRRK2 R1441G/K17A/K18A (red) was transfected into HeLa cells plated on collagen coated coverslips and stained and localized with pRab10 (green) as in A. (C) Quantification of pRab10 overlap with LRRK2 by Mander's coefficient. Error bars represent SEM of means from three different experiments (represented by colored dots), each with >40 cells per condition. Significance was determined by *t* test, *P = 0.0108.

Figure 7. LRRK2 K17 and K18 increase pRab10 recovery after LRRK2 inhibitor washout. (A-D) FLAG-LRRK2 R1441G, FLAG-LRRK2 R1441G/K17A/K18A, LRRK2, or LRRK2 K17A/K18A was transfected into HeLa cells. 48 hr post transfection cells were treated with 200nM of MLi-2 for 1 hr. The MLi-2 was then removed by multiple washes and incubated for the indicated times prior to cell lysis. Whole cell extracts (20µg) were subjected to quantitative immunoblot analysis using anti-LRRK2, anti-LRRK2 pS935, anti-Rab10, and anti-pRab10 antibodies. (E-F) Quantification of pRab10/ total Rab10 fold change and normalized to no MLi2 control. Error bars represent mean ± SD from 2 different experiments per condition.

Figure 8. Feed-forward pathway for Rab10 phosphorylation is dependent on LRRK2 kinase activity. (A) Fluorescence intensity traces of individual, single molecules of 7nM CF633-labeled FLAG-LRRK2 R1441G on a substrate supported lipid bilayer across 600 sec of live TIRF microscopy. Red, R1441G; Blue, K17A/K18A/R1441G; Yellow, D2017A. B. Reactions were carried out as in (A) except Rab10 was omitted (purple) or Rab10 was replaced with Rab11 (green). Dashed lines in A and B represent time of addition of fluorescently labeled LRRK2 at 60 sec. Fluorescence intensity was fitted by a nonlinear regression curve for two phase association. Fold change was calculated by

dividing the average fluorescence intensity at steady state and subtracting background fluorescence intensity average determined from 60 sec prior to LRRK2 addition. C. Rate of membrane association of LRRK2 as a function of Rab10 concentration. This curve was fitted by a nonlinear regression fit using PRISM software (Mathworks) to determine a Hill coefficient.

Figure 9. A model for LRRK2 membrane recruitment. See text for details.

Supporting VIdeos

Movie 1. TIRF microscopy of R1441G LRRK2 binding to Rab10-lipid bilayers

Movie 2. TIRF microscopy of R1441G LRRK2 binding to lipid bilayers without Rab10

Movie 3. TIRF microscopy of R1441G LRRK2 binding to Rab11-lipid bilayers

Movie 4. TIRF microscopy of D2017A LRRK2 binding to Rab10-lipid bilayers

Movie 5. TIRF microscopy of K17A/K18A/R1441G LRRK2 binding to Rab10-lipid bilayers

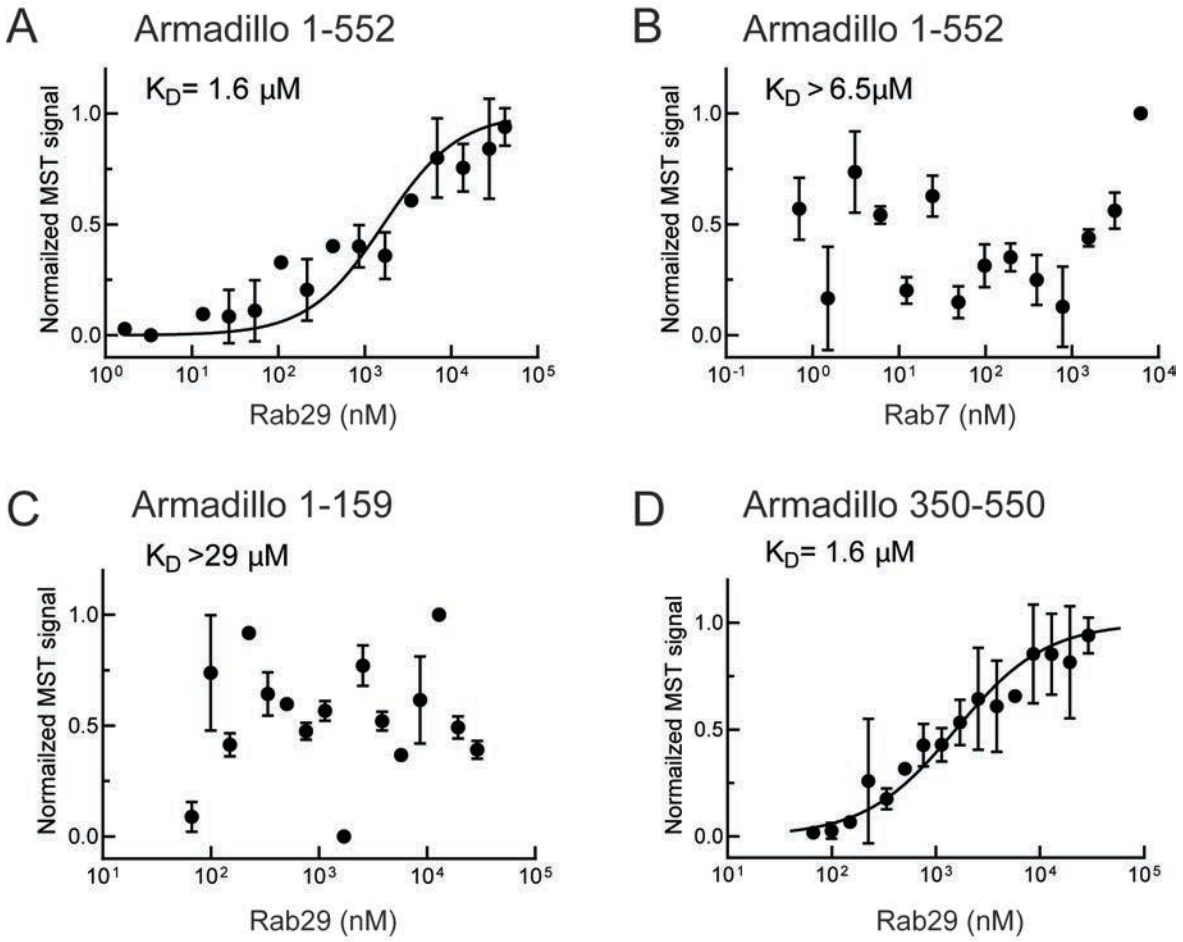

Vides et al., Figure 1

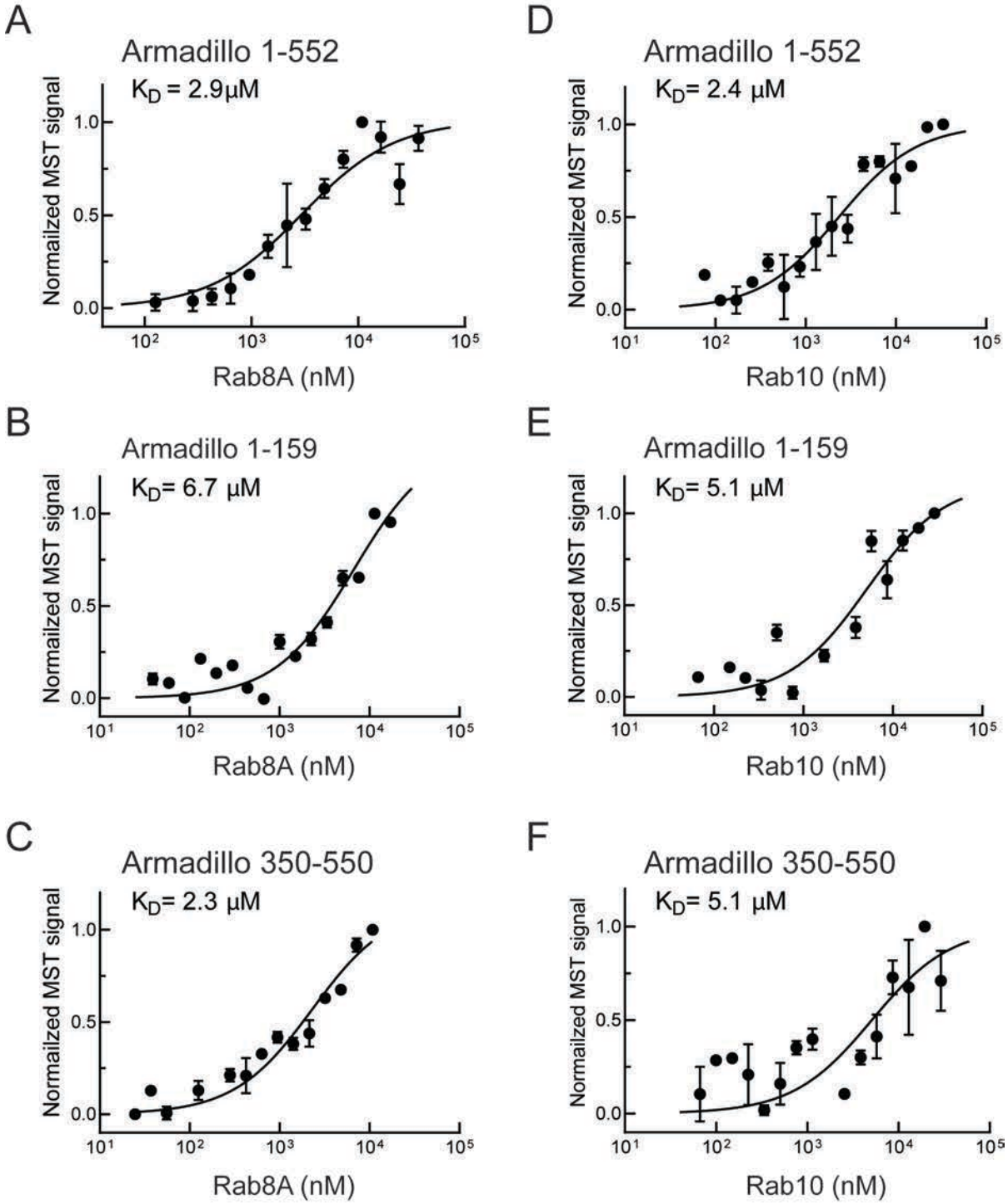

Vides et al., Figure 2

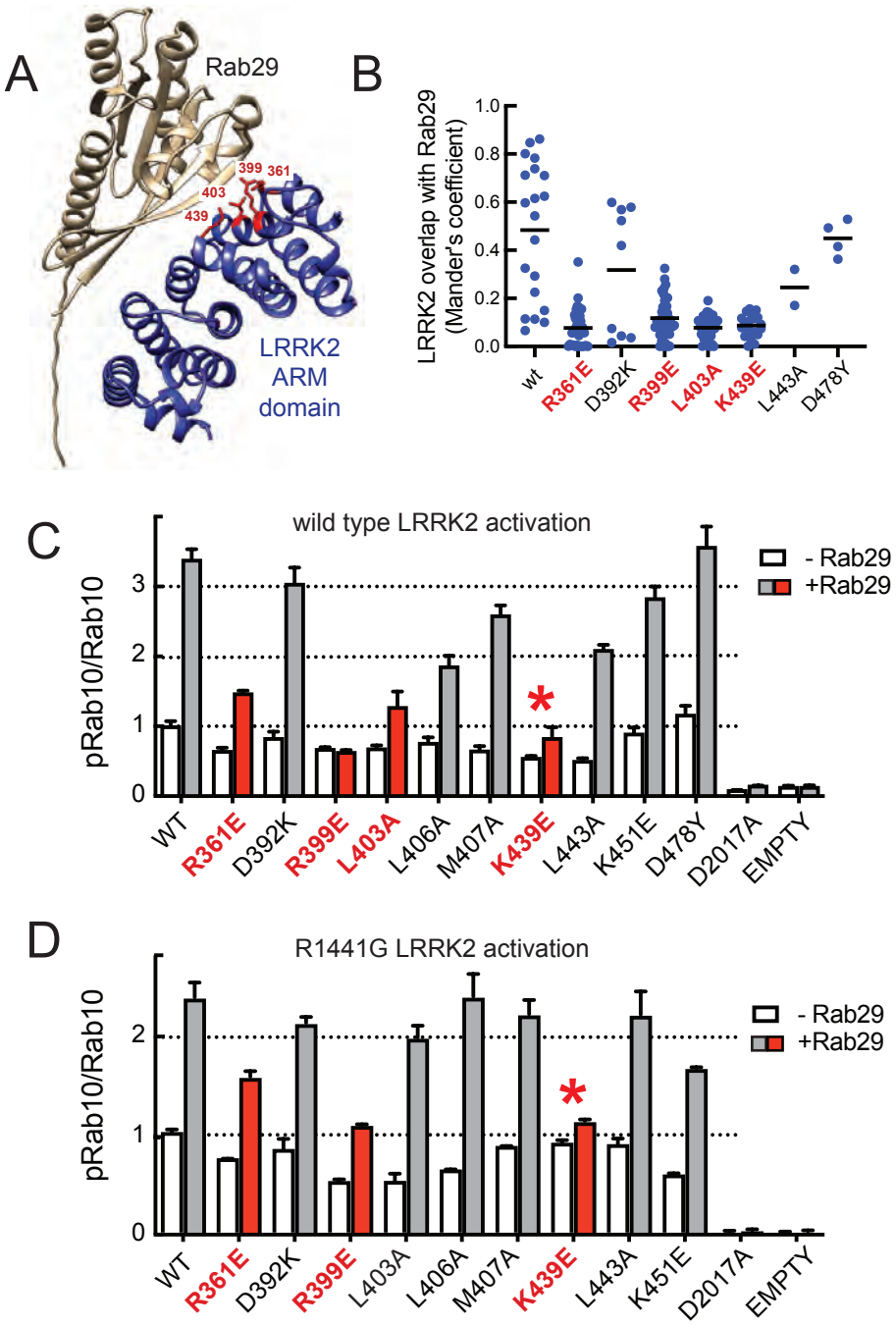

Vides et al., Figure 3

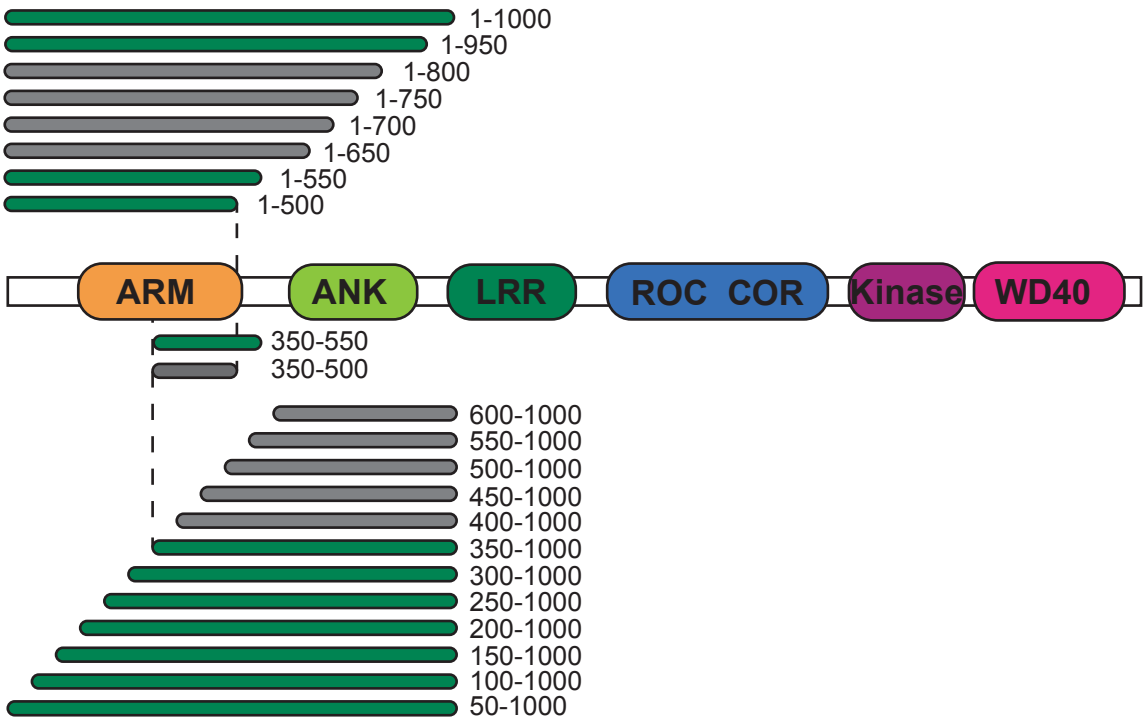

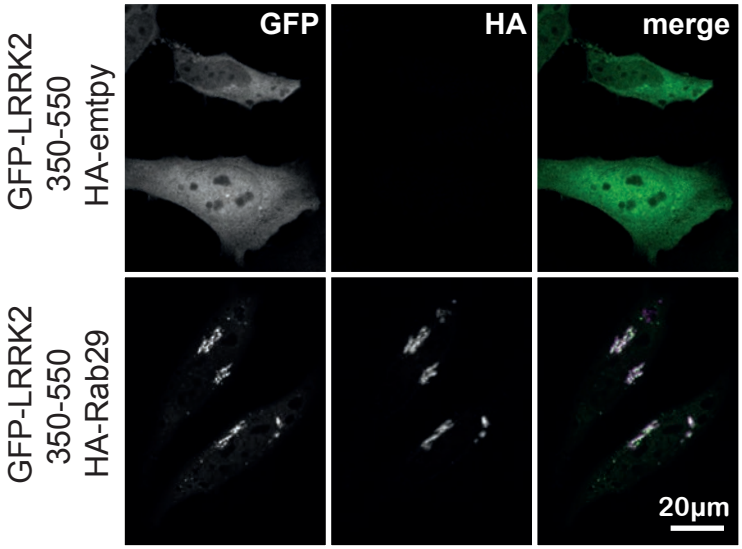

Vides et al. Figure 3 -- Figure Supplement 1

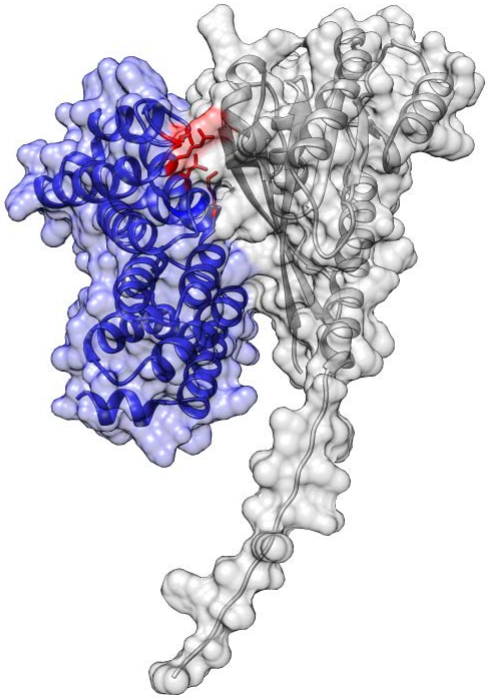

LRRK2 (350-550)	Rab29	Distance (Å)	Interaction
R361	Y77	3.07	hydrogen bond
R361	Y77	2.99	hydrogen bond
R361	M73	4.68	hydrophobic
K362	S72	2.48	hydrogen bond
K362	L76	4.44	hydrophobic
D392	K37	3.38	H bond, electrostatic, salt bridge
R399	D43	4.21	electrostatic
L403	V42	5.01	hydrophobic
L406	W62	5.36	hydrophobic
M407	L76	4.99	hydrophobic
M407	Y77	4.73	hydrophobic
K439	D43	3.24	H bond, electrostatic, salt bridge
K439	F44	3.22	hydrogen bond
K439	F44	5.23	hydrophobic
L443	R58	5.30	hydrophobic
K451	D80	4.92	electrostatic

Vides et al., Figure 3 -- Figure Supplement 2

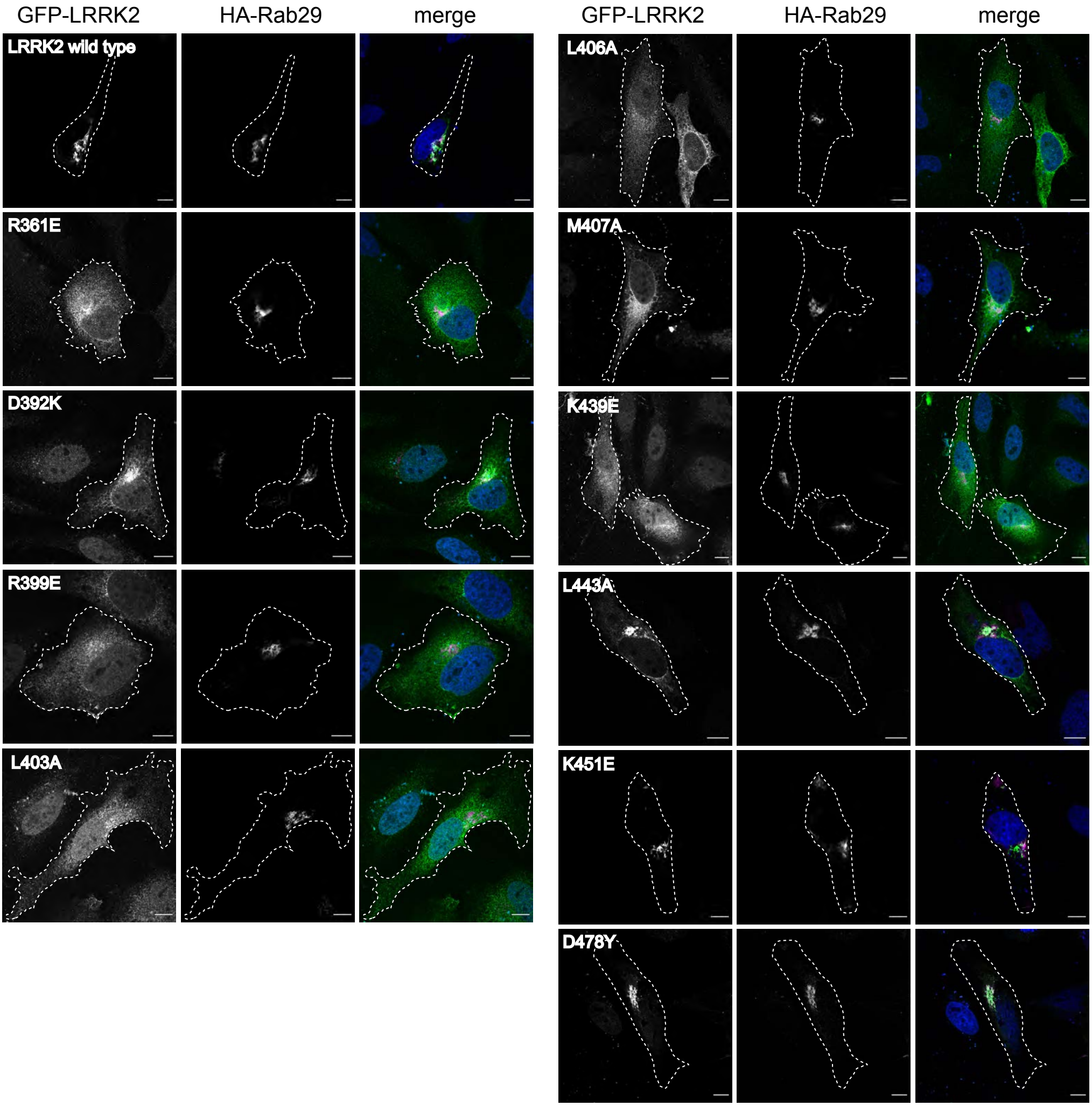

Vides et al., Figure 3 -- Figure Supplement 3

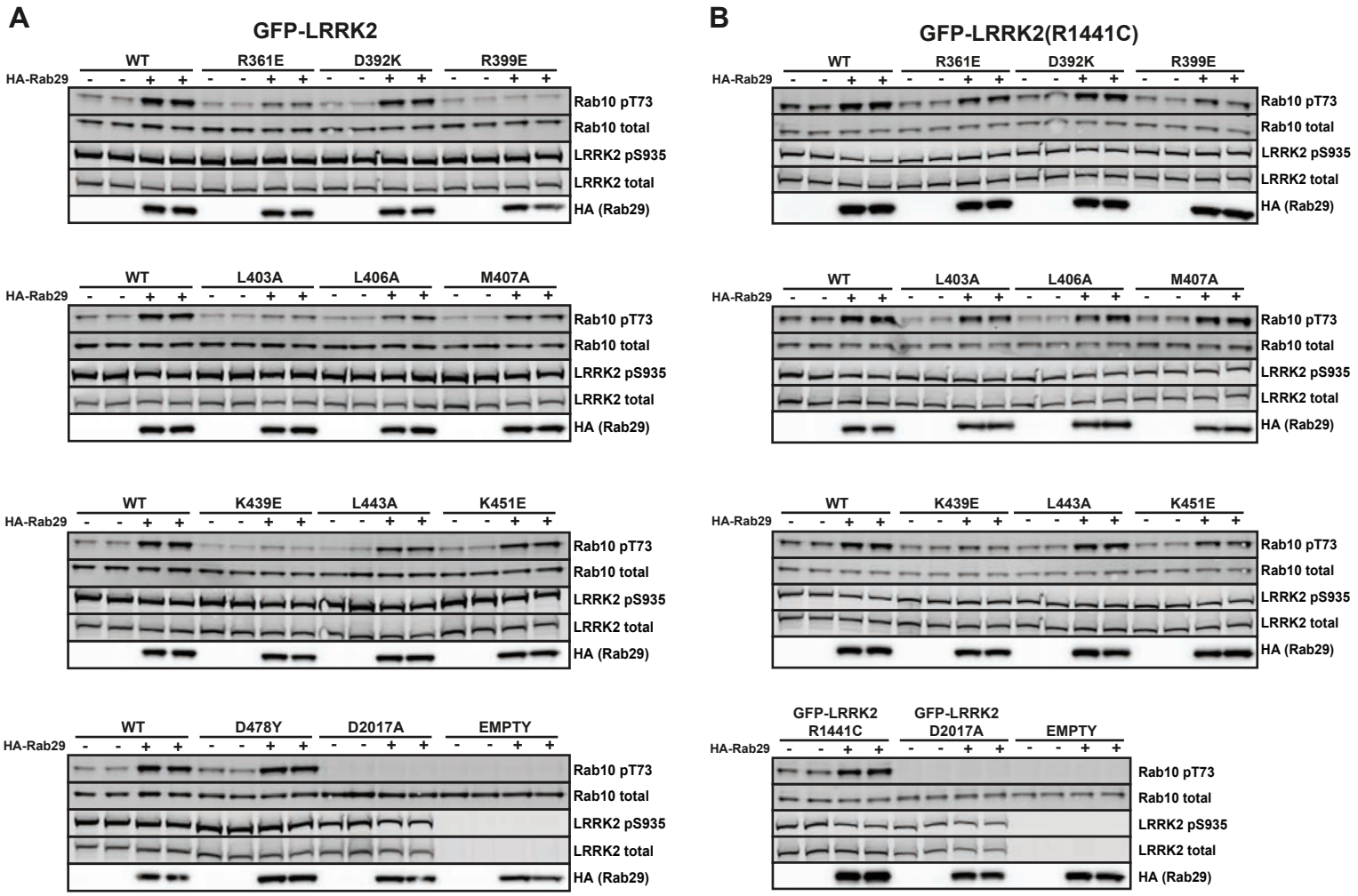

Vides et al. Figure 3--Fig. Supp. 4

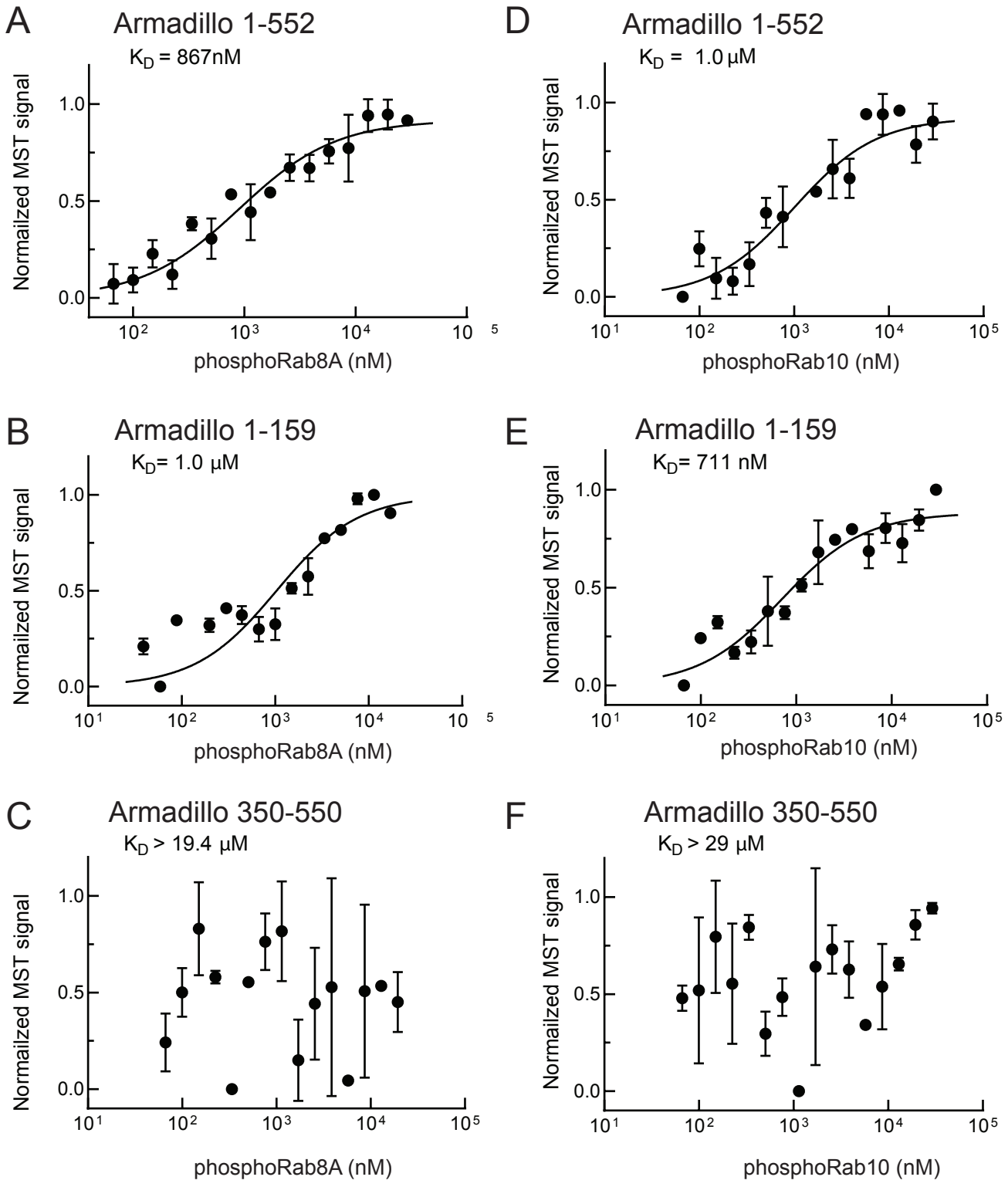

Vides et al., Figure 4

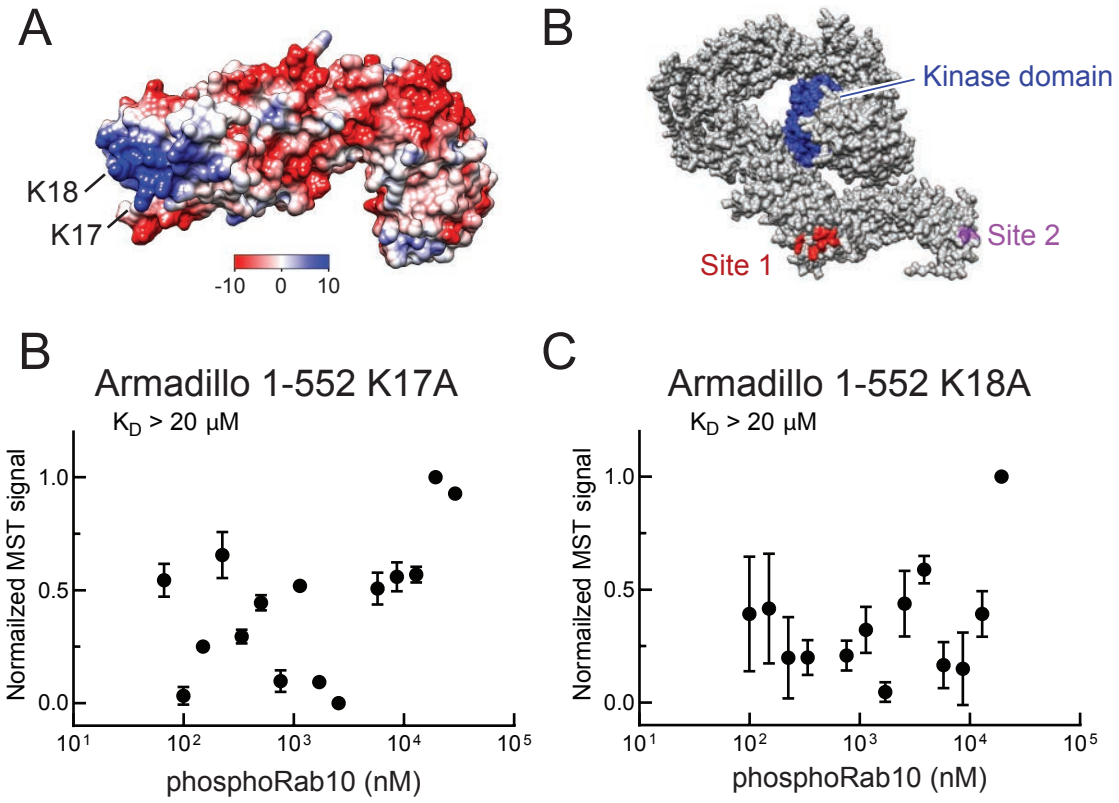

Vides et al., Figure 5

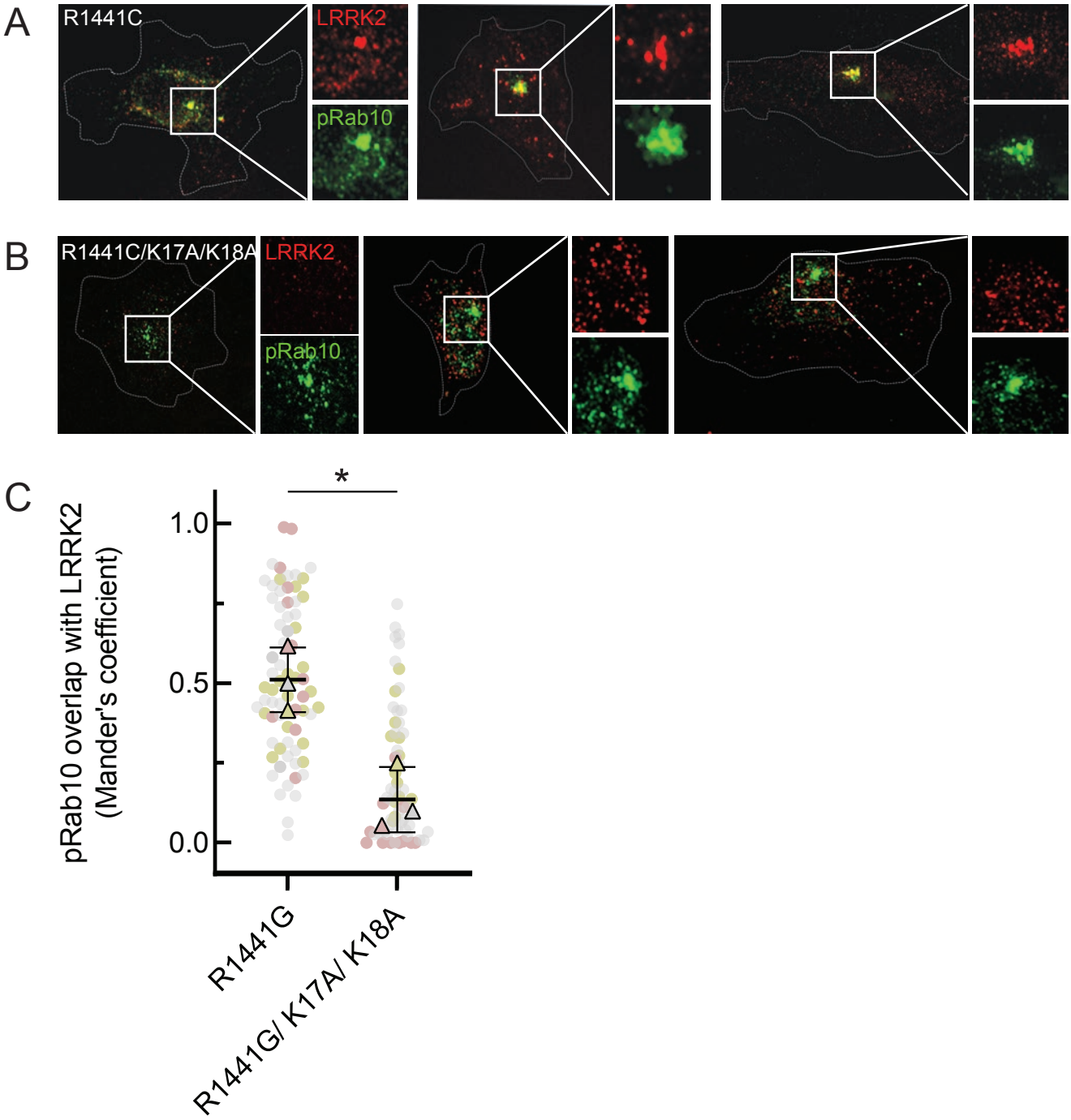

Vides et al., Figure 6

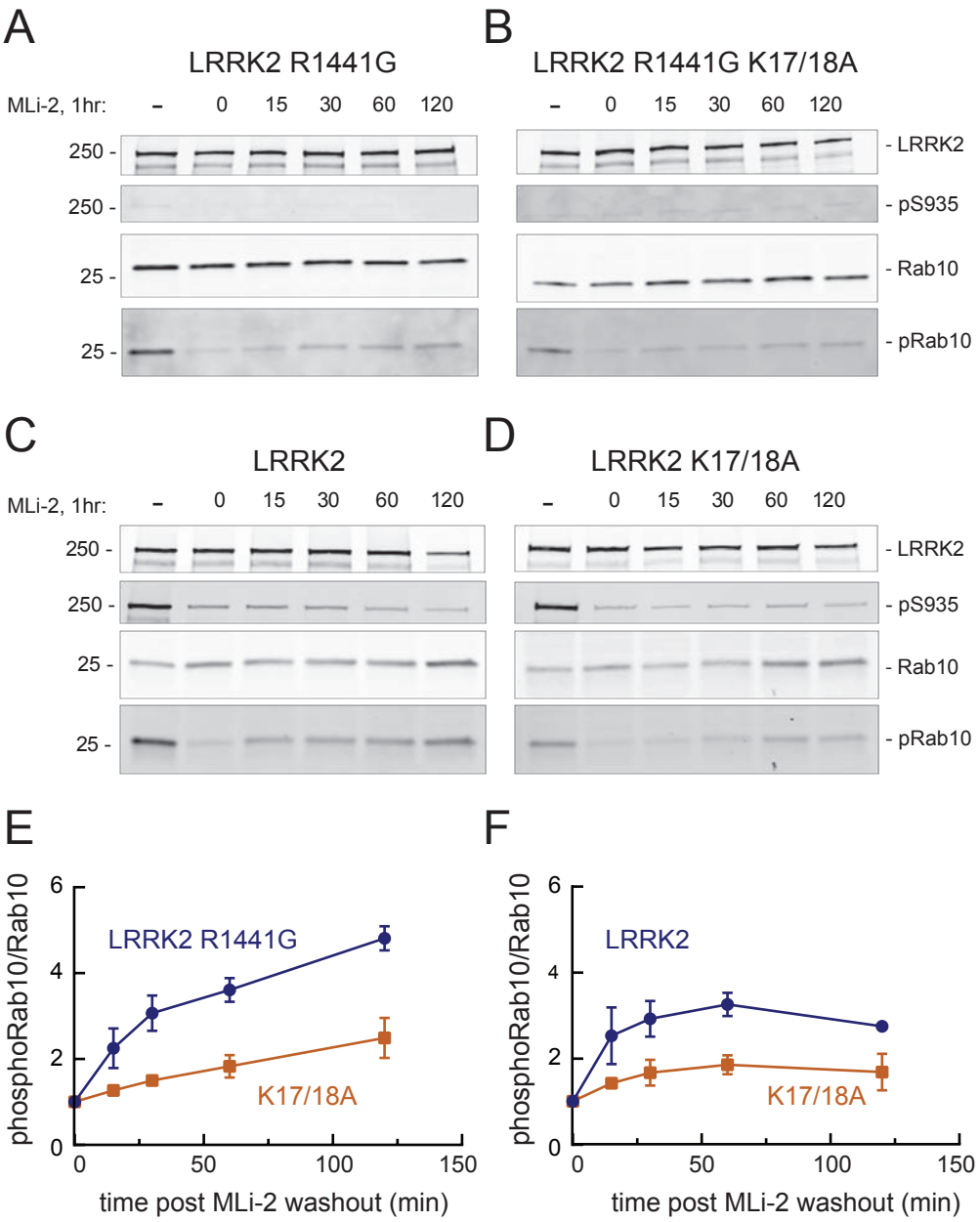

Vides et al., Figure 7

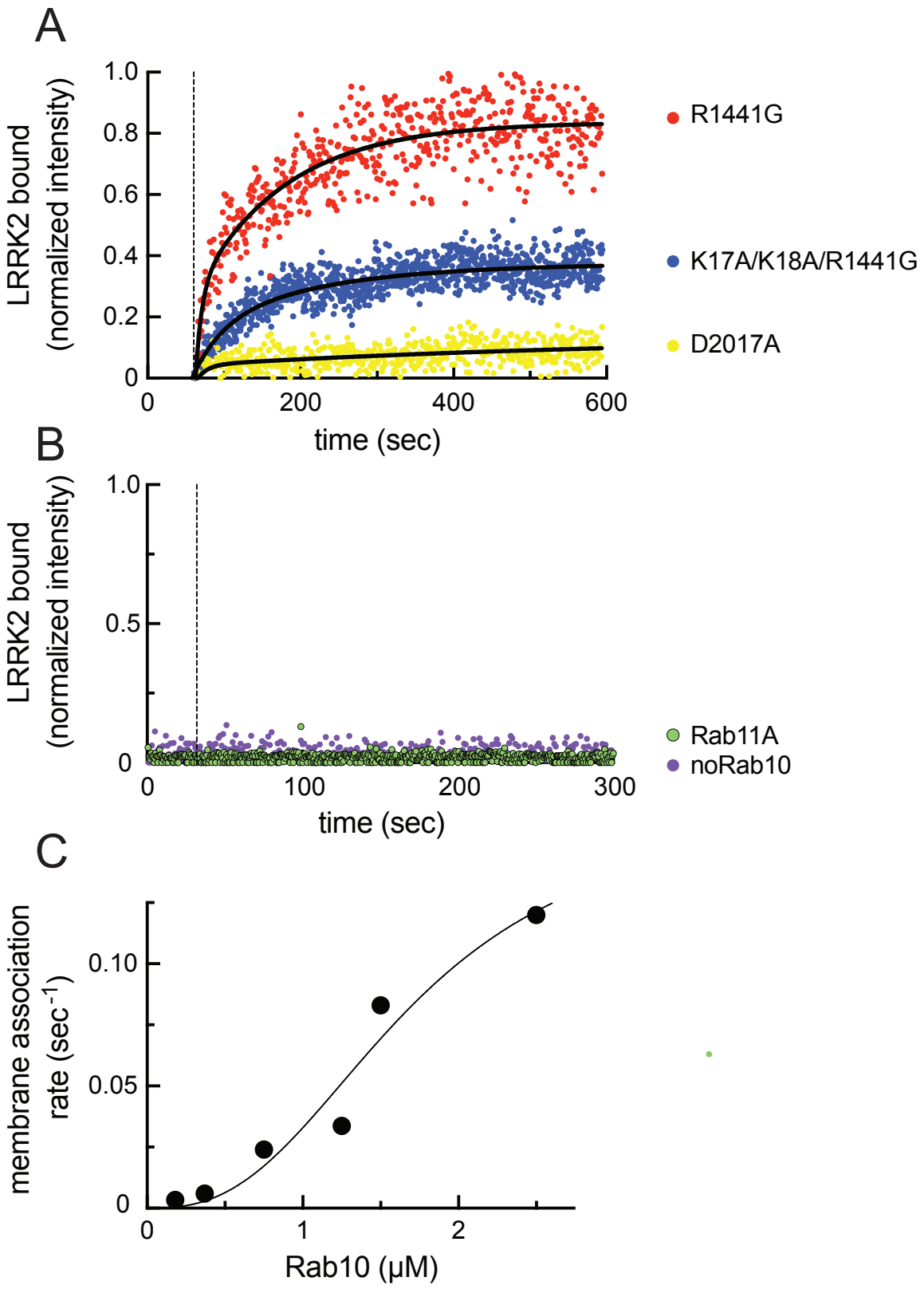

Vides et al., Figure 8

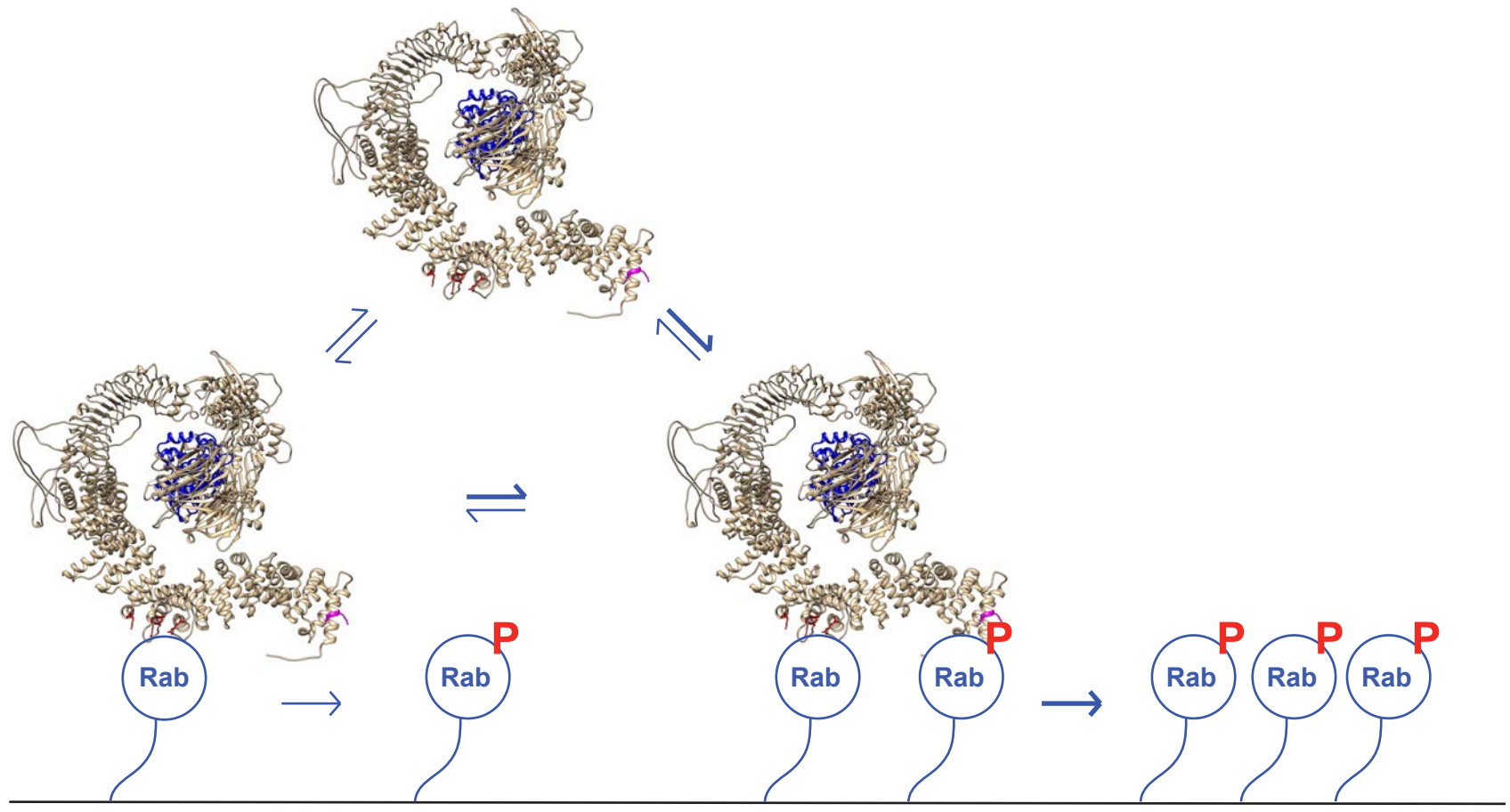

Vides et al., Figure 9